4.11 Membrane Technology for Water: Microfiltration, Ultrafiltration, Nanofiltration, and Reverse Osmosis

AG Fane, CY Tang, and R Wang, Nanyang Technological University, Singapore

Nomenclature

a	molecular radius
A	water permeability coefficient (solution-diffusion model)
A_m	membrane area
B	solute permeability coefficient (solution-diffusion model)
C	solute concentration
$\bar{C}$	average solute concentration inside the membrane

C_b	bulk concentration	Q_p	volumetric flow rate that permeates through the membrane
C_f	feedwater concentration		
C_i	molar concentration of dissolved species i	r_p	pore radius
C_m	solute concentration near the membrane surface	R	rejection
		R_{app}	apparent rejection of a membrane
C_p	solute concentration in the permeate water	Re	Reynolds number
		R_f	foulant hydraulic resistance
C_{wm}	concentration of water inside the RO rejection layer	R_g	universal gas constant $(R = 8.31 \, \text{J} \, \text{mol}^{-1} \, \text{K}^{-1})$
d_h	hydraulic diameter	R_{int}	intrinsic rejection of a membrane
D	diffusion coefficient of solute	R_m	membrane hydraulic resistance
D_{sm}	diffusion coefficient of solute inside the RO rejection layer	R_{sys}	overall rejection – or rejection at a system level
D_{wm}	diffusion coefficient of water inside the RO rejection layer	S	specific surface area
		Sc	Schmidt number
J_{crit}	critical flux	Sh	Sherwood number
J_s	solute flux	T	absolute temperature (K)
J_w	water flux	u	flow velocity
K	mass transfer coefficient	v	kinetic viscosity
K_{KC}	Kozeny–Carman coefficient	V_w	molar volume of water
K_{sm}	solute partitioning coefficient into the RO rejection layer	Y	recovery
		ε	membrane porosity
l_m	thickness of the rejection layer	λ	ratio of solute (or particle) diameter to the pore diameter
L_p	water permeability		
L_s	solute permeability coefficient	η	viscosity of water
$\dot{m}_s$	solute mass flow rate	δ	boundary layer thickness
M_w	molecular weight	π	osmotic pressure
P	hydraulic pressure	π_m	osmotic pressure at the membrane surface
P_m	hydraulic pressure near the membrane surface	π_p	osmotic pressure of the permeate water
		σ	reflection coefficient
P_p	hydraulic pressure of the permeate water	τ	tortuosity of the membrane

4.11.1   Introduction

Membrane technology is used in the water industry to improve the quality of water for use, reuse, or discharge to the environment. Membranes range from finely porous structures to nonporous and can remove contaminants such as bacteria and protozoa down to ions. The advantages of membrane technology include its modular nature, allowing application at very large or small scale, the quality of the product water, the relatively small footprint, and, in some cases, the lower energy usage. Increased water scarcity, coupled with steady improvements in membrane performance, costs, and energy demand, will see a steady growth in membranes in the water industry into the foreseeable future.

4.11.1.1   The Range of Membrane Processes

Membranes used for purification and separation can be defined as semipermeable thin films. The semipermeable property means that membranes may be able to transport water but not bacteria (microfilters) or salts (reverse osmosis, RO). Other membranes are able to transport salts but not water (electrodialysis). The family of membrane processes is depicted in Figure 1 which shows the driving force for transport

and the size range of the species involved. For driving forces ΔC and ΔE, the species transported are solutes and water transport is low. For the liquid-phase pressure-driven processes (ΔP), water is transported and other species are partially or wholly retained. Gas-phase separations are also possible, such as N_2/O_2 or CO_2/CH_4, and details can be found elsewhere (Hagg, 2008). Membrane distillation (MD) is a process driven by temperature difference (ΔT) using hydrophobic membranes with vapor-filled pores. The ΔT provides a vapor pressure driving force for water vapor transport; a detailed review can be found elsewhere (Khayet, 2008).

The membrane processes of interest in the water industry are the pressure-driven liquid-phase processes summarized in Table 1. The microfiltration/ultrafiltration (MF/UF) range can be regarded as a continuum. These membranes are typically produced by phase inversion, and small changes in preparation technique adjust the nominal pore size. The nanofiltration/reverse osmosis (NF/RO) membranes also represent a continuum and are usually produced as thin-film composite (TFC) structures. Section 4.11.2 gives details of the various types of membrane and their properties. Section 4.11.3 describes membrane preparation and Section 4.11.4 shows how membrane properties are characterized. Section 4.11.5 explains the role of the membrane module (housing) and
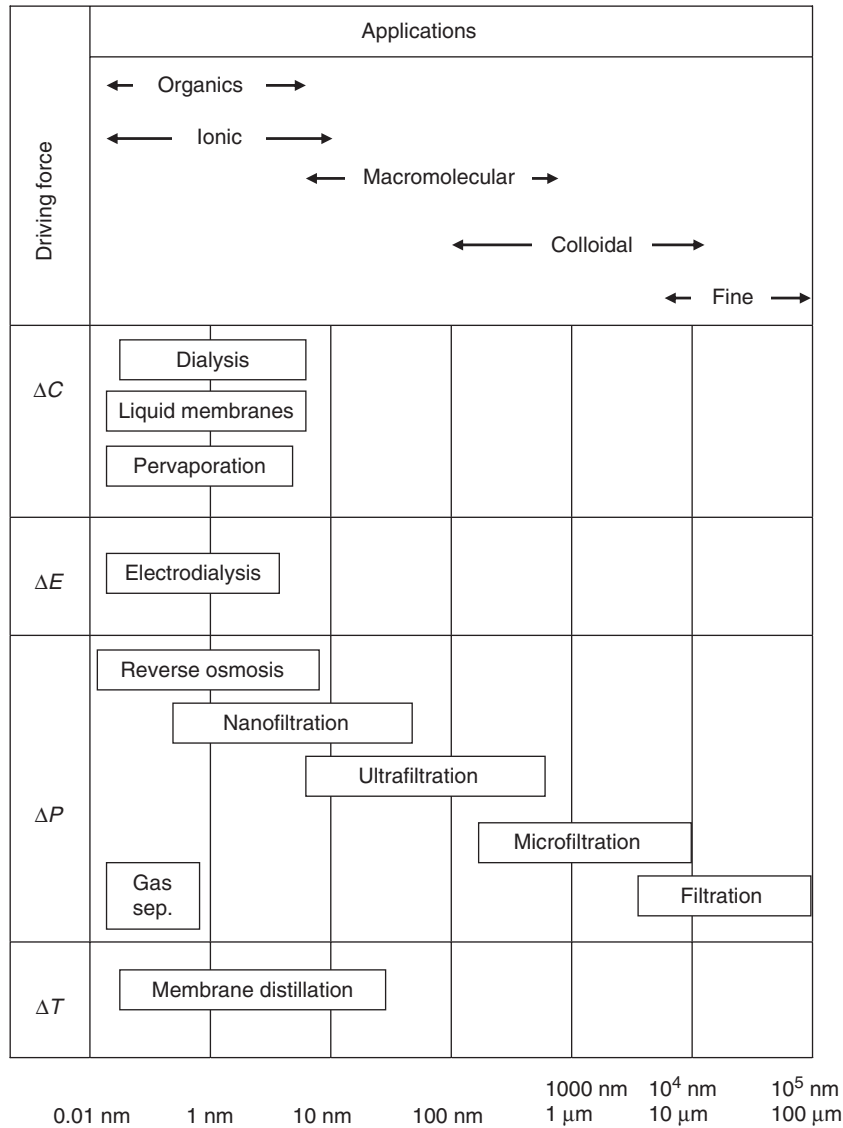
Figure 1   The family of membrane processes (driving forces and applications size range).

Table 1   Typical properties of pressure-driven membranes

	Microfiltration	Ultrafiltration	Nanofiltration	Reverse osmosis
Pore size (nm)	50–10 000	1–100	~2	<2
Water permeability ($l\,m^{-2}\,h^{-1}\,bar^{-1}$)	>500	20–500	5–50	0.5–10
Operating pressure (bar)	0.1–2.0	1.0–5.0	2.0–10	10–100
MWCO (Da)	Not applicable	1000–300 000	>100	>10
Targeted contaminants in water	Bacteria, algae, suspended solids, turbidity	Bacteria, virus, colloids, macromolecules	Di- and multivalent ions, natural organic matter, small organic molecules	Dissolved ions, small molecules
Membrane materials	Polymeric, inorganic	Polymeric, some inorganic	Thin-film composite polyamide, cellulose acetate, other materials (Schafer et al., 2005)	Thin-film composite polyamide, cellulose acetate

Adapted from Winston and Sirkar (1992) and Mulder M (1996) *Basic Principles of Membrane Technology*, 2nd edn. Dordrecht: Kluwer.

introduces the various module types. Section 4.11.6 provides the basic relationships describing membrane performance.

4.11.1.2   Role in Water Supply, Sanitation, and Reclamation

The needs of the water industry (water supply, sanitation, and reclamation) are to remove various contaminants to make the water fit for purpose. Potable water requires removal of pathogens, organic species, and salts to specify limits. Some industrial waters have even tighter limits, for example, boiler feedwater, or ultrapure water for microelectronics. Wastewater treatment, such as sanitation, involves biological treatment and subsequent polishing. Water reclamation takes treated wastewater and upgrades it to high quality for industry or indirect potable reuse (IPR). Industrial water applications are very broad but could encompass water treatment to industry standards, water recovery and recycle, and treatment for discharge. It will be evident that the pressure-driven liquid-phase membrane processes, with the properties given in Table 1, provide the means to achieve the above separations. In many cases, the membrane process is used in combination with another unit operation (such as a bioreactor) in a hybrid membrane process. In other cases, low-pressure (MF/UF) membranes are used as pretreatment to high-pressure (NF/RO) membranes in dual membrane processes.

Figure 2 is a simplified generic flow sheet of a membrane process as applied in the water industry. In addition to the membrane separation, it is not uncommon to have both pretreatment and posttreatment steps. It should also be noted that contaminant removal inevitably results in reject (waste) streams that have to be dealt with. Input streams may also be involved in pre- and posttreatment. The following are brief descriptions of water industry applications of membranes. Table 2 summarizes the membrane process configurations for the range of applications and water sources.

4.11.1.2.1   Water treatment

Table 2 identifies five water treatment applications (WT.1–WT.5), based either on low-pressure MF/UF membranes in hybrid processes or on tighter NF membranes. The water sources involved are low salinity. WT.1 is the most typical configuration for membrane-based water treatment plant (Kennedy et al., 2008); the posttreatment may be simpler depending on the natural organic matter (NOM) removal achieved upstream. Disinfection by chlorine is usually applied to maintain a residual in the distribution system. The low-pressure membranes are predominantly hollow fibers, either contained or submerged (see Section 4.11.5). In most applications the suspended solid content of the source is relatively low and this allows operation in dead-end mode (see Section 4.11.7), with cycles of filtration and backwash, typically over 30–60 min. The WT.2 option, combining membranes and powdered activated carbon (PAC), is used in cases where the
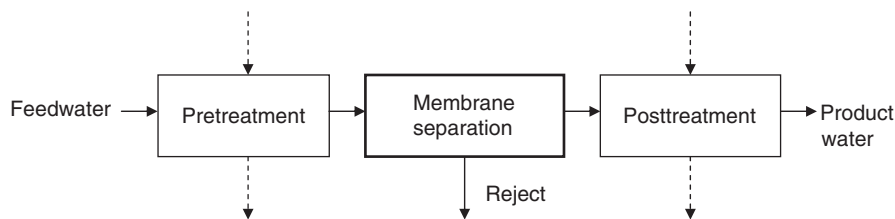

Figure 2   Generic flow sheet of membrane process.

Table 2   Membrane process configurations in the water industry

Application	Source water	Membrane process	Pretreatment or hybrid	Posttreatment	Target removals
Water treatment					
WT.1	Surface	MF/UF	Coagulation	AOT, BAC, Dis	NOM, turbidity, pathogens
WT.2	Surface	MF/UF	PAC	Dis	Taste/odor, trace organics
WT.3	Surface	NF	Filtration	Dis	NOM
WT.4	Surface	NF	Coagulation + filtration	AOT	Trace organics, taste/odor
WT.5	Ground	NF	Filtration	Dis	Hardness
Desalination					
D.1	Brackish ground	RO	Filtration	Dis	Salinity
D.2	Seawater	RO	Media filtration or MF/UF	Ca addition	Salinity
Reclamation					
R.1	Treated wastewater	RO	MF/UF	AOT	Pathogens, trace organics
R.2	Wastewater	RO	MBR	AOT	Pathogens, trace organics
Membrane bioreactor					
MBR.1	Wastewater	MF/UF	Screening	Dis	BOD, turbidity, pathogens

AOT, advanced oxidation treatment (UV, etc.); BAC, biologically active carbon; BOD, biochemical oxygen demand; Dis, disinfection (chlorination, etc.); MBR, membrane bioreactor; MF, microfiltration; NOM, natural organic matter; PAC, powdered activated carbon; UF, ultrafiltration.

water may encounter trace organics or taste and odor (Lebeau et al., 1998).

Applications WT.3–5 use NF membranes on low-salinity surface- or groundwaters. NF operates at higher pressures than MF/UF and also requires crossflow to control fouling, rather than dead-end operation, and consequently has a higher energy demand. WT.3 is popular in Norway (Wittmann and Thorsen, 2005), where raw waters are high in NOM and energy is relatively plentiful. WT.4 makes use of the ability of NF to remove organics of 100–200 Da size, and is exemplified by the treatment of river water in France to remove trace herbicides (Wittmann and Thorsen, 2005). In some locations, NF is also used on groundwater to remove calcium hardness.

4.11.1.2.2   Desalination

Saline water sources range from brackish groundwater to seawater. In these applications, the key membrane process is RO. The role of pretreatment is to protect the RO membranes from various foulants (see Section 4.11.6.5), and posttreatment prepares the product water for discharge. Application D.1 (Table 2) is brackish water desalination. These are usually modest-size plants for local water supplies. A major challenge for this application is how to dispose of the plant reject and which is a high-salinity stream. Various options are available (Voutchkov and Semiat, 2008), including evaporation ponds and subsurface disposal.

Application D.2 is desalination of seawater, which is effectively a limitless source. In this case, the high salinity and high osmotic pressure require an operating pressure of 60–70 bar, making seawater reverse osmosis (SWRO) more energy intensive than the other membrane/water options. Pretreatment has to be able to minimize various forms of fouling (inorganic, organic, and biofouling). Most SWRO plants with feedwater from ocean intakes opt for either media filtration, or increasingly use low-pressure membranes for pretreatment. In the case of SWRO, the reject (brine) stream is typically 50% of the intake flow, and is discharged back into the ocean, subject to adequate arrangements for rapid dispersion of salinity. Prior to discharge, the pressurized brine passes through energy recovery devices which can recover >95% of the pressure energy in the brine for pressurizing a portion of the feed. The product water is usually conditioned by addition of calcium ions to satisfy World Health Organization (WHO) requirements (Cote et al., 2008). A detailed description of desalination by RO is given in Voutchkov and Semiat (2008).

4.11.1.2.3   Water reclamation

Municipal wastewater provides the second limitless source of water. Reclamation processes convert secondary effluent (R.1 in Table 2) or raw wastewater (R.2) into water of exceptionally high quality. Process R.1 is more common as it builds on the existing municipal wastewater infrastructure. Secondary effluent has relatively low suspended solids, total organic carbon (TOC), and salinity, which makes it very attractive as a source water. It also tends to be located close to where it could be reused. All major reclamation plants use dual membrane arrangements with the low-pressure (MF/UF) pretreatment membranes operating in dead-end cycles, similar to MF/UF water treatment plant, and providing very low solids feed to the RO. Due to the low-salinity feed, the RO operates at much lower pressures and with higher recoveries (75% vs. 50%) than SWRO. This means that the reclamation plant can produce high-quality water at approximately half the energy and costs of SWRO (see Section 4.11.7.3). A comprehensive review of membrane reclamation plant and comparison with SWRO can be found elsewhere (Cote et al., 2008). Posttreatment in R.1 is typically ultraviolet (UV) which provides an added barrier to virus and also oxidizes trace organic compounds, possibly present at ppb levels in the RO permeate. Flow sheet option R.2 uses a membrane bioreactor (MBR, see Section 4.11.1.2.4) in place of the conventional activated sludge processes (CASPs) combined with MF/UF. This option would probably be favored in a green field site due to the smaller foot print and the reported better-quality feed (lower TOC) to the RO (Cote et al., 2008). The high-quality water produced by the dual membrane reclamation process is suitable for demanding industrial applications and for IPR.

4.11.1.2.4   Wastewater MBR

The CASP combines a wastewater bioreactor and a settling tank. The membrane bioreactor (MBR) replaces the settling tank with low-pressure membranes. The advantages of the MBR include an improved effluent quality (solids-free, potentially lower TOC) and significantly smaller foot print. The membrane separation allows the biomass mixed liquor to be increased to 10–$20\,\mathrm{g\,l^{-1}}$, compared with the $<5\,\mathrm{g\,l^{-1}}$ in the CASP. This improves organics removal and can reduce the excess waste sludge for disposal. Typically, MBRs operate with mixed liquors of 10–$12\,\mathrm{g\,l^{-1}}$, which is a compromise to avoid raised viscosity that would impair oxygen transfer. MBRs have either submerged (immersed) membranes in the bioreactor, or external side-stream membranes connected so that mixed liquor can be cycled through the modules. Submerged membranes use either hollow fibers in bundles (or curtains) or flat sheets, vertically aligned, operated under suction. Side-stream modules use large bore hollow fibers. Pretreatment for MBRs is usually fine screening to eliminate sharp objects that could damage the membranes. Posttreatment depends on the fate of the permeate, but at a minimum it would involve disinfection.

Membrane fouling (see Section 4.11.6.5) is a major challenge in MBRs, due to the complex nature of the mixed liquor with its biomass floc, colloids, and macrosolutes. Fouling is mitigated by careful selection of the operating flux and by maintaining a vigorous crossflow induced by air sparging below the membranes or in the membrane loop. A comprehensive review of MBR fouling is available (Le-Clech et al., 2006). More detailed information on MBRs can be found in Judd (2006) and Lieknes (2009).

4.11.1.3   Status of Development

Membrane technology in the water industry has grown from a research curiosity to mainstream applications over a brief period of 50 years. This section outlines the major developments and milestones and summarizes the status of the various applications.

4.11.1.3.1   Seawater desalination

The application of membranes in the water industry started in the 1960s, following the invention of the cellulose acetate (CA) RO membrane by Loeb and Sourirajan (1964). The CA-RO membrane was an alternative to thermal desalination of seawater and brackish water to provide drinking water. Over the next two decades, seawater RO steadily developed, but was considered relatively costly and energy intensive, suitable for niche applications. A major advance occurred in the late 1970s with the invention of the TFC membrane (see Section 4.11.3.3) by Cadotte (1977). The TFC significantly improved both water flux and salt retention and has become the basis for modern SWRO membranes. The ability to tune the chemistry of the TFC separating layer has allowed steady improvements in performance.

Both CA-RO and TFC-RO membranes are produced in continuous flat sheets. The housing, or module (see Section 4.11.5) developed to package these membranes, is the spiral-wound module (SWM). This is produced in standard sizes, typically 8 in (203 mm) diameter and 40 in (1016 mm) long, which allows interchange between products. Over the 30-year period from 1978 to 2008, the SWM has steadily improved, with a drop in real cost (1/12), an increased life (2.3 ×), an improved water production rate (2.5 ×), and a reduced salt transmission (1/7) (Birkett and Truby, 2007). The SWM is now the module of choice for RO, NF (and some large-scale UF in other industries). However from the mid-1960s to the late 1990s, there were two SWR options, one the SWM, the other the hollow fiber RO membrane produced by Dupont and others. The HFRO was initially predominant in larger-scale SWRO plant. However, the SWM became more competitive because of the better performance of the TFC membrane, its slightly lower pretreatment requirements, and its evolution into an interchangeable standard module. The SWM is now the predominant option for large SWRO and reclamation plant. Current (2010) trends are to larger 16-in-diameter SWMs with 4 × the water output per element. Membrane developments include the thin-film nanocomposite (TFNC), which incorporates highly permeable zeolite nanoparticles into its separation layer (Jeong et al., 2007). Energy demand and costs for SWRO have steadily declined (see Section 4.11.7), largely due to the introduction of high-efficiency energy recovery devices that recover the pressure energy in the RO concentrate stream. Desalination capacity by SWRO now exceeds that of thermal processes. Plant capacities of several hundreds of ML d^{-1} are not uncommon and applications continue to grow due to increasing water scarcity and population growth.

4.11.1.3.2   Water reclamation

Water reclamation with membranes commenced at a significant scale in the 1970s with Water Factory 21 in Orange County California. This plant took secondary-treated municipal effluent and used physical/chemical pretreatment prior to RO. Today, this plant uses low-pressure membrane (UF) pretreatment as do all the major reclamation plants. Water reclamation processes provide significant augmentation of water supplies in some locations. For example, the Singapore NeWater plants (Seah et al., 2008) provide about 20% of Singapore's water supply. The high-quality water produced by water reclamation plant tends to go to industrial usage, with a portion going to IPR. The likely trend will be for more membrane-based IPR schemes, due to lower cost and energy demand than SWRO and increased confidence in its water quality.

4.11.1.3.3   Water treatment

Water treatment with low-pressure membranes is now well established, but the growth only started in the early 1990s. Prior to this, membranes were considered too expensive for the production of a low-cost product, such as water – the exception being SWRO in niche areas. Several factors have contributed to the rapid growth in low-pressure membrane water treatment, including tighter treatment standards in the US prompted by a serious cryptosporidium outbreak in 1993, a concerted effort by manufacturers to reduce membrane plant costs and the adoption of dead-end with backwash operation (see Section 4.11.7.1) with lower energy demand. The current low-pressure membrane options are hollow fibers either in submerged or in pressurized modules (see Section 4.11.5), and both concepts appear to be equally popular. There is a small, but growing, interest in the use of ceramic membranes for water treatment, particularly in Japan. Claimed benefits are higher fluxes and longer membrane lifetimes. Higher-pressure NF membranes are also well established for effective removal of hardness and organic contaminants, including trace pollutants such as herbicides and endocrine disruptors (EDCs). NF is a more expensive option than low-pressure UF or MF, but has application in special cases (Wittmann and Thorsen, 2005).

4.11.1.3.4   Membrane bioreactors

MBRs for wastewater treatment have been around since the late 1960s. In the early period, a major incentive was to increase the biomass mixed liquor (MLSS) to high levels (>20 g l^{-1}) to reduce excess sludge production. However, this exacerbated fouling and reduced oxygen transfer. In addition, the high cost of membranes favored relatively high fluxes that required vigorous crossflow and high-energy input to control fouling. As a result, the MBR was another niche membrane application until the early 1990s. The significant growth in MBRs has been due to innovations in design and operation. First, the lower cost of membranes allowed a lower design flux with less intrinsic fouling. Second, the use of a two-phase flow, such as bubbling, has been found to control fouling with substantially reduced energy costs. Third, the use of submerged (immersed) membranes provided an alternative MBR configuration, besides allowing retrofitting to existing plants.

The current status is that MBR applications are becoming widespread in industry and increasingly in municipal use. There tend to be more, but smaller, plant in industry and some large (>100 ML d^{-1}) municipal plant (Lieknes, 2009). MBR designs are not standardized and popular options include submerged membranes, with either hollow fibers or flat sheets, or pressurized side-stream vessels with hollow fibers. All applications use the two-phase flow to control fouling. While current MBRs are all aerobic processes, there is a significant R&D effort in anaerobic MBRs (AnMBRs), with the

incentive of energy recovery in biogas. Future applications of AnMBRs can be anticipated.

4.11.2 Membrane Types and Properties

A pressure-driven membrane is a selective barrier for separation. Its selectivity and permeability depend strongly on its pore characteristics (pore size, pore-size distribution, and porosity). Thus, membrane pore structure is one of the most important properties affecting membrane performance. Depending on the pore structure, pressure-driven membranes can be classified into RO, NF, UF, or MF membranes. Other important membrane properties include membrane hydrophilicity, surface charge, roughness, etc. These properties are discussed in this section.

4.11.2.1 Membrane Types and Important Membrane Properties

Membrane pore structure is one of the most important properties of a membrane, as this largely determines the selectivity as well as the permeability of a membrane. Pressure-driven membranes can be classified into porous and nonporous membranes on the basis of membrane pore size (Table 1). MF and UF membranes are porous membranes that can be operated at low pressures. For this reason, MF and UF membranes are also frequently referred to as low-pressure membranes. The pore structure of MF and UF membranes can be observed using an electron microscope. In contrast, the rejection layer of a typical RO membrane does not appear to have any visible pores under an electron microscope. RO membranes are believed to be nonporous. In some literature, subnanometer pore size is reported for RO membranes based on their rejection properties of dissolved ions and small organic molecules. Finally, an NF membrane is an intermediate between a tight UF membrane and a loose RO membrane. Both RO and NF membranes require relatively high operating pressure, and they are also referred to as high-pressure membranes.

The performance parameters and pore size range for MF, UF, NF, and RO membranes are summarized in Table 1:

- MF membranes typically have pore sizes ranging from 0.05 to 10 μm. Corresponding to their relatively large pore sizes, MF membranes have high permeability ($>500\,l^{-1}\,m^{-2}\,h^{-1}\,bar^{-1}$) and can be operated in a low-pressure range (typically from 0.1 to 2.0 bar). MF membranes are used to retain particulates whose size is greater than membrane pore size. They can be fabricated from both polymeric and inorganic materials with either symmetric or asymmetric structures (Figure 3). For symmetric MF membranes, the pore diameters do not vary over the entire cross section of the membrane, and the thickness of the membrane determines its flux. Depending on the manufacturing method used, MF can also be asymmetrically structured, but the pores of the active layer are not much smaller than those of the supporting substructure.

- UF membranes have pore sizes ranging from 1 to 100 nm. This pore size range allows them to be used for removing bacteria, viruses, colloids, and macromolecules from a feedwater. The selectivity of a UF membrane is commonly represented by its molecular weight cutoff (MWCO), which is defined as the molecular weight of the solute that achieves a 90% rejection by the membrane. The MWCO of typical UF membranes is in the range of 1–300 kDa. A larger MWCO indicates that the membrane has a lower rejection ability and that it has a larger pore size. The MWCO of a membrane can be used to determine the pore size of the membrane by relating the molecular radius (a) of the solute molecules to its molecular weight (M_w):

$$a = 0.33 M_w^{0.46} \tag{1}$$

(valid for dextran, a in Å and M_w in Da, from Aimar et al. (1990)).

UF membranes typically have an asymmetric structure (Figure 3) to maximize its membrane permeability. A very thin (0.1–1 μm) active or selective skin layer with fine pores is supported by a highly porous 100–200-μm-thick substructure. The pore diameters may increase from one side of the membrane (the skin layer) to the other (supporting sublayer) by a factor of 10–1000 (Strathmann, 1990). Its separation characteristics and mass flux are determined mainly by the feature of the skin layer (pore size, pore-size distribution and thickness, etc.), while the porous sublayer serves only as a mechanical support. Because of such an asymmetric structure, UF membranes gain excellent separation performance and considerable strength from the fine pore size of the thin active layer, and encounter little mass transfer resistance from the open supporting substructure. Typical permeability ranges from 20 to $500\,l\,m^{-2}\,h^{-1}\,bar^{-1}$. The normal operating pressure ranges from 1.0 to 5.0 bar.

- RO membranes are able to remove small organic molecules and dissolved ions, including monovalent ions such as Na^+ and Cl^-. These membranes have subnanometer pores and their separation properties are generally reported in terms of water permeability and sodium chloride rejection. They
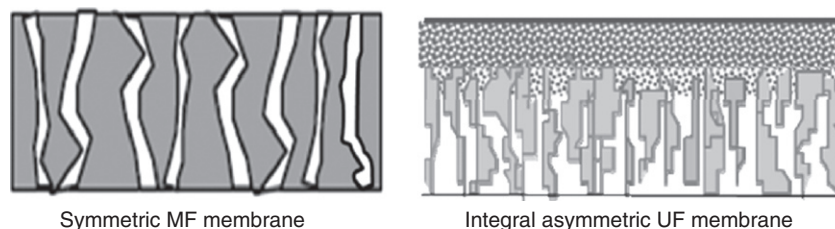

Symmetric MF membrane   Integral asymmetric UF membrane

Figure 3 Structures of symmetric and asymmetric membrane. MF, microfiltration; UF, ultrafiltration.

can be further subdivided into SWRO membranes and brackish water RO (BWRO) membranes. SWRO membranes are used for seawater desalination, and they generally have high sodium chloride rejection (>99%). Such high rejection is typically achieved using a highly crosslinked dense rejection layer which tends to have a low water permeability ($<1 l m^{-2} h^{-1} bar^{-1}$). High pressure (>60 bar) is required for SWRO operation to overcome the osmotic pressure of seawater as well as the large hydraulic resistance of the membrane. Compared to SWRO membranes, BWRO membranes have lower sodium chloride rejection (>95%) but higher water permeability (1–10 $l m^{-2} h^{-1} bar^{-1}$). Relatively lower operating pressure (10–20 bar) is required. Some BWRO membranes are marketed as low-energy or high-flux RO membranes.

- NF membranes are similar to RO membranes in that they can retain dissolved ions as well as some small organic molecules. The difference between NF and RO is that NF membranes typically have low rejection to monovalent ions such as Na^+ (10–90%). The rejection of dissolved ions depends strongly on their valence, and divalent and multivalent ions tend to be better rejected. Due to their ability to effectively remove calcium and magnesium ions, NF membranes can be used for water softening. Many NF membrane manufacturers also provide rejection data on solutes other than sodium chloride, such as magnesium chloride, magnesium sulfate, or glucose. NF membranes can be operated at significantly lower pressure levels (<10 bar) compared to those for RO membranes due to their higher water permeabilities (5–50 $l m^{-2} h^{-1} bar^{-1}$).

There are two types of structure for RO and NF membranes. One is an integral asymmetric structure formed by the phase-inversion method, and the other is a TFC structure formed by interfacial polymerization method (see Section 4.11.3.3). An integral asymmetric RO/NF membrane is made of one polymer material and has a thin, permselective skin layer with a thickness of 0.1–1 μm supported by a more porous sublayer. The membrane's flux and selectivity are determined by the dense skin layer, while the porous sublayer has little impact on the membrane separation properties. In contrast, a TFC RO/NF membrane is made of two or more polymer materials. The most important TFC composite membranes are made from crosslinked aromatic polyamide by the interfacial polymerization method, on a microporous polymer such as polysulfone (PS) support layer, followed by a reinforcing fabric (see Section 4.11.2.2).

In addition to the membrane separation properties, other important membrane properties include the following.

Chemical, mechanical, and thermal stability. A good membrane shall be mechanically stable. For many applications, pH, temperature, and chlorine tolerance are important considerations. For example, RO membranes synthesized from CA are susceptible to hydrolysis and biodegradation. These membranes can only be used within a narrow pH and temperature range, which is one of the major causes for phasing out of this type of RO membrane. Modern RO membranes are typically based on polyamide chemistry with a TFC structure. Unfortunately, TFC RO membranes have low chlorine resistance (Kwon et al., 2006, 2008). Where chlorine disinfection is needed for biofouling control, the free chlorine level needs to be carefully controlled to prevent unacceptable membrane damage.

Hydrophilicity. A hydrophilic membrane is water like, that is, water has a strong affinity to its surface and it has a tendency to wet the surface. In contrast, a hydrophobic membrane does not interact favorably with water. The relative hydrophilicity/hydrophobicity can be determined by contact-angle measurements (Section 4.11.4). In general, a hydrophilic membrane surface is preferred as it tends to enhance water permeability and reduces membrane fouling propensity. A hydrophobic membrane is preferred for some special applications (such as MD and some membrane contactors) where transmission of liquid water through the membrane needs to be prevented.

Surface charge. A membrane surface can gain surface charge due to either its charged functional groups or preferential adsorption of some specific ionic species. For example, most TFC polyamide RO membranes are negatively charged at neutral pH due to the presence of carboxylic groups ($-COO^-$) (Tang et al., 2007a). Membrane surface charge plays an important role in fouling. A positively charged particle may have a strong tendency to deposit on a negatively charged membrane surface due to electrostatic attraction (Jones and O'Melia, 2000). In addition, rejection of ionic species as well as membrane permeability can be affected by surface charge for RO, NF, and tight UF membranes as a result of electrostatic interaction (Donnan exclusion effect; see Schafer et al. (2005)). For example, Childress and Elimelech (2000) reported that both salt passage and water flux were maximum at the pore isoelectric point (~pH 5) for an NF membrane. Membrane surface charge has also been used to correlate the transport of some trace organic solutes (Kimura et al., 2003).

Surface roughness. Surface roughness has been reported as an important parameter for RO and NF membrane fouling. A rougher membrane surface tends to promote fouling likely due to reduced shear force over the membrane surface and increased membrane nonhomogeneity (e.g., nonuniform flux distribution over a membrane surface) (Vrijenhoek et al., 2001; Tang and Leckie, 2007).

4.11.2.2 Membrane Properties for RO and NF Membranes

The physiochemical properties, such as surface roughness, hydrophobicity, and rejection properties, of RO and NF membranes strongly depend on the chemistries forming these membranes (Petersen 1993; Tang et al., 2007a, 2009a, 2009b). There are mainly two types of RO membranes in the market: (1) asymmetrical CA-RO membranes formed by phase inversion and (2) TFC polyamide RO membranes formed by an interfacial polymerization process (Petersen, 1993). CA membranes, though they have hydrophilic and smooth membrane surfaces, have low resistance to hydrolysis and biodegradation. In addition, their separation properties (permeability and rejection) are inferior to modern TFC-PA membranes. A comparison between typical CA and polyamide RO membranes is presented in Table 3. Both CA and polyamide can be used to form NF membranes. In addition, other polymers (e.g., polyvinyl alcohol (PVA) and sulfonated PS) and inorganic materials (e.g., some metal oxides) can also be

Table 3   Comparison between cellulose acetate (CA) and thin-film composite (TFC) reverse osmosis (RO) membranes

Parameter	CA RO membrane	TFC polyamide RO membrane
Permeability	Low	High ($\sim 5\,l\,m^{-2}\,h^{-1}\,bar^{-1}$ for brackish water RO)
NaCl rejection (%)	85–98	95–99.9
Surface hydrophilicity	Very hydrophilic	Less hydrophilic
Surface roughness	Smooth	Rough surface with valley-and-ridge structures
Maximum temperature (°C)	30	45
Stable pH range	4.5–6.5	3–10 (2–11 for some membranes, e.g., with a polyvinyl alcohol surface coating)
Resistance to hydrolysis	Low. Unstable at pH < 4.5 or pH > 6.5, and accelerated hydrolysis at high temperature	Good
Chlorine resistance	Stable at low levels (< 1 ppm)	Low tolerance to free chlorine (< 0.1 ppm)
Resistance to biodegradation	Low	Relatively good

Polyamide ~ 0.05 − 0.3 μm

Polysulfone ~ 20−50 μm

Backing layer ~ 200 μm
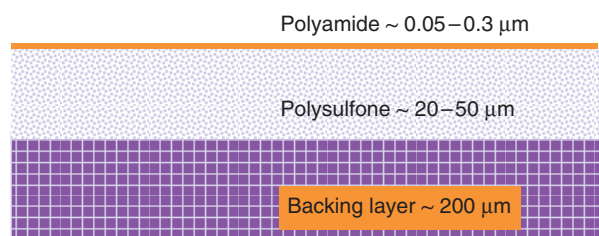
Figure 4   Schematics of a thin-film composite polyamide membrane. The composite PA membrane typically comprises three distinct layers – a thin, dense selective layer (the polyamide layer) of 50–300 nm in thickness, a polysulfone support layer of 20–50 μm in thickness, and a nonwoven fabric backing layer.

used for NF synthesis. A thorough review of RO and NF chemistry is available elsewhere (see Petersen (1993)) for RO and (Schafer et al., 2005) for NF membranes. The current section focuses on the structure and properties of TFC polyamide RO and NF membranes (Petersen, 1993).

A typical TFC polyamide membrane comprises a dense polyamide rejection layer of ∼ 100 nm in thickness on top of a microporous PS or polyethersulfone (PES) support (Figure 4). The PS/PES layer, typically casted on a nonwoven fabric layer of 100–200 μm in thickness, provides a mechanical support to the rejection layer. Among the three layers, the polyamide rejection layer is the most critical one, as most of the membrane properties (e.g., permeability, rejection, surface charge, roughness, and surface hydrophilicity) are determined by this ultrathin dense rejection layer (Tang et al., 2007a; Petersen, 1993). In addition, the mechanical properties of the different layers are important, as RO and NF membranes need to withstand high pressures. The PS or the polyamide layer may deform mechanically and become more compact under high pressure. This reduces the membrane permeability with time, a phenomenon known as membrane compaction.

Most commercial TFC-RO membranes for water treatment are formed by interfacial polymerization of aromatic amine

monomers (such as *m*-phenylenediamine (MPD) in an aqueous solution) and aromatic acid chloride monomers (such as trimesoyl chloride (TMC) in an organic solvent). Since the discovery of this reaction scheme by Cadotte and the development of the first commercial fully aromatic TFC RO membrane FT30 by FilmTec©, the reaction scheme and its variations have been widely used to prepare most commercial TFC-RO membranes (Petersen, 1993). In general, fully aromatic TFC RO membranes formed in this way have a high degree of crosslinking (i.e., the fraction of crosslinked repeating units; see Figure 5) (Tang et al., 2007a). Increased crosslinking tends to increase salt rejection but decrease water permeability. Commercial BWRO membranes (e.g., XLE from Dow FilmTec and ESPA3 from Hydranautics) have a water permeability in the range of $4–8\,l\,m^{-2}\,h^{-1}\,bar^{-1}$ and sodium chloride rejection > 95% (Table 4). Seawater RO membranes have lower water permeability but much higher salt rejection (> 99%). It is worth noting that rejection of a solute (R) is not an inherent property of an RO membrane, as it also depends on the operating conditions such as applied pressure. A more fundamental property of a nonporous RO membrane is the solute permeability coefficient (B). The NaCl permeability coefficient is also tabulated in Table 4 for some commercial RO membranes. The solute permeability coefficient can be determined from rejection test results via

$$B = A(\Delta P - \Delta \pi)(R^{-1} - 1) \qquad (2)$$

Typical fully aromatic polyamide RO membranes formed by TMC and MPD have rough membrane surfaces, with a root-mean-square (RMS) roughness (ridge-and-valley) on the order of 100 nm (Table 4). The surface is negatively charged at neutral pH due to the deprotonation of carboxylic (–COOH) functional group (Tang et al., 2007a; Childress and Elimelech, 1996). The typical contact angle for an unmodified membrane is 40–50°.

Some posttreatment steps, such as the application of a coating layer or additives, might be involved to protect the
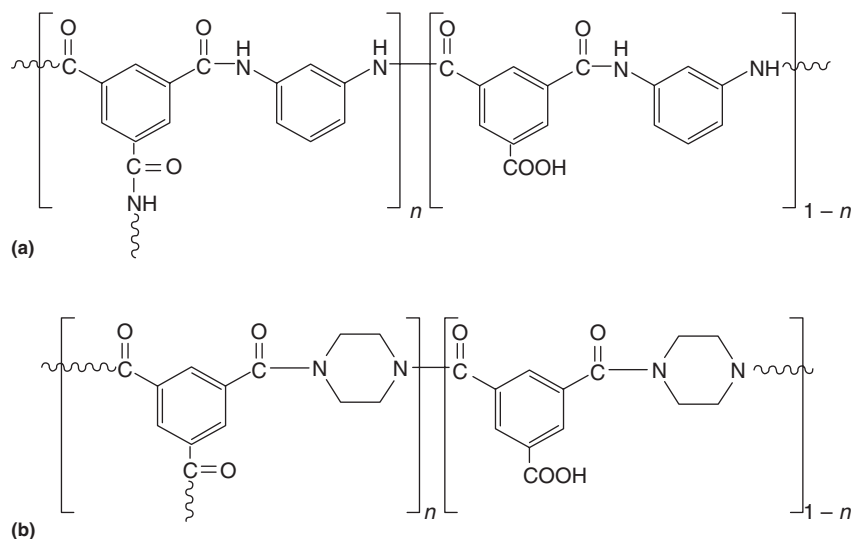
Figure 5 Typical chemistry for interfacially formed TFC-RO and NF membranes. (a) Fully aromatic polyamide based on trimesoyl chloride and *m*-phenylenediamine. (b) Semi-aromatic polyamide based on trimesoyl chloride and piperazine. Modified from Tang CY, Kwon YN, and Leckie (2009b) Effect of membrane chemistry and coating layer on physiochemical properties of thin film composite polyamide RO and NF membranes. I. FTIR and XPS characterization of polyamide and coating layer chemistry. *Desalination* 242: 149–167; and Petersen RJ (1993) Composite reverse-osmosis and nanofiltration membranes. *Journal of Membrane Science* 83: 81–150.

Table 4   Physiochemical properties of thin-film composite (TFC) polyamide reverse osmosis (RO) and nanofiltration (NF) membranes

Chemistry	Type	Membrane	A $(l\,m^{-2}\,h^{-1}\,bar^{-1})^a$	B for NaCl $(l\,m^{-2}\,h^{-1})$	R for NaCl $(\%)^a$	RMS roughness (nm)	Contact angle (°)	Zeta potential (mV) at pH 9
MPD + TMC, no coating	SWRO	SWC4	0.80	0.11	99.0	135.6	48.8	−20.9
	BWRO	XLE	6.04	3.02	96.5	142.8	46.4	−27.8
	BWRO	LE	4.29	2.60	95.8	95.7	47.2	−26.1
	BWRO	ESPA3	7.52	5.58	94.9	181.9	43.1	−24.8
MPD + TMC, PVA coating	SWRO	SW30HR	0.85^b	0.11^b	99.6^b	54.4	30.9	−1.7
	BWRO	LFC1	3.96	1.52	97.3	135.8	20.1	−13.2
	BWRO	LFC3	2.81	0.59	98.5	108.4	22.8	−6.5
	BWRO	BW30	3.96	1.17	97.9	68.3	25.9	−10.1
MPD + TMC, no coating	NF	NE90	9.04	11.6	91.5	72.4	46.3	−21.0
	NF	NF90	11.2	9.17	94.4	129.5	44.7	−37.0
PIP + TMC, no coating	NF	HL	12.8	653	21.3	7.2	27.5	−26.0
	NF	NF270	14.5	152	56.9	9.0	32.6	−41.3

[a]The permeability of all membranes except BW30 was evaluated using ultrapure water at an applied pressure of 1380 kPa (200 psi). Rejection of all membranes except BW30 was determined using a 10 mM NaCl solution at pH 7.

[b]The permeability and rejection for BW30 was calculated from the membrane manufacturer's specification. The testing pressure for BW30 was 55 bar for a feedwater containing 32 000 mg l^{-1} NaCl.

MPD, *m*-phenylenediamine; PIP, piperazine; RMS, root-mean-square; TMC, trimesoyl chloride.

Adapted from Tang CY, Kwon YN, and Leckie JO (2009a) Effect of membrane chemistry and coating layer on physiochemical properties of thin film composite polyamide RO and NF membranes II. Membrane physiochemical properties and their dependence on polyamide and coating layers. *Desalination* 242: 168–182.

membrane surface and/or improve membrane properties. Membrane surface properties, such as hydrophilicity and surface charge density, are largely determined by the top-most layer. Consequently, the application of a surface coating can greatly affect these properties. For example, PVA, a neutral and hydrophilic polymer, has been widely used for coating RO membranes to achieve improved membrane properties. The PVA-coated RO membranes are less rough and less charged (Table 4). They are significantly more hydrophilic, with a contact angle of only 20–30° (Table 4 and Figure 6), and thus they are expected to be less prone to membrane fouling. Many commercial membranes marketed as low-fouling composite RO membranes are PVA coated. Some examples are the low fouling composite (LFC) series from Hydronautics and

BW30 from Dow FilmTec (Tang *et al.*, 2009a). Commerical PVA-coated membranes tend to have better rejection than uncoated ones, but their permeability is lower probably due to the additional hydraulic resistance from the coating layer (Tang *et al.*, 2009a). Other commonly used coating materials and additives reported in the literature include poly(ethylene oxide-*b*-amide) (Pebax®), chitosan, and sodium alginate (Schafer *et al.*, 2005; Louie et al., 2006).

Similar to TFC RO membranes, TFC NF membranes can be formed by the fully aromatic polyamide chemistry (such as MPD reacting with TMC). Some commercial examples include NF90 from Dow FilmTec and NE90 from Saehan Industries. With a less crosslinked polyamide compared to typical RO membranes, these TFC-NF membranes have lower sodium chloride rejection ($\sim$90–95%) and higher water permeability of about $10\,l\,m^{-2}\,h^{-1}\,bar^{-1}$. Similar to fully aromatic RO membranes, MPD+TMC-based NF membranes have negatively charged membrane surfaces with ridge-and-valley type of roughness. Their contact angle is also similar to MPD+TMC-based RO membranes.

Some other TFC-NF membranes are semi-aromatic where an aliphatic amine monomer is used with the aromatic TMC (Petersen, 1993). The most widely used amine monomer for semi-aromatic TFC-NF membranes is piperazine (PIP) (Petersen, 1993; Schafer *et al.*, 2005). Some commercial examples of PIP+TMC-based NF membranes include NF270 from Dow FilmTec and HL from GE Osmonics. Poly (piperazinamide) NF membranes have higher fluxes, lower rejections, and smoother and more hydrophilic membrane surfaces than fully aromatic NF membranes. In Table 4, it is apparent that there is a strong trade-off between water permeability and salt rejection – a more water permeable membrane tends to have lower rejection and higher solute permeability.

4.11.2.3 Membrane Properties for MF and UF Membranes

Porous MF and UF membranes can be formed by a wide range of structures, materials, and formation methods (refer to Section 4.11.3). Therefore, the properties of MF and UF membranes can vary significantly. By far, the most important consideration for porous membrane selection is the pore structure (e.g., pore size, pore-size distribution, porosity, tortuosity, and thickness of the active separation layer), as their flux and retention properties are mainly determined by these properties. In addition, membrane flux and rejection can be marginally affected by some material properties, including hydrophilicity. In general, hydrophilic membranes are preferred due to their lower fouling tendency and higher water permeability.

There are many different pore structures for porous membranes (Figure 7). A track-etched MF membrane typically has straight cylindrical pores. These pores are perpendicular or slightly oblique to the membrane surface. The membrane permeability for cylindrical-pore membranes can be
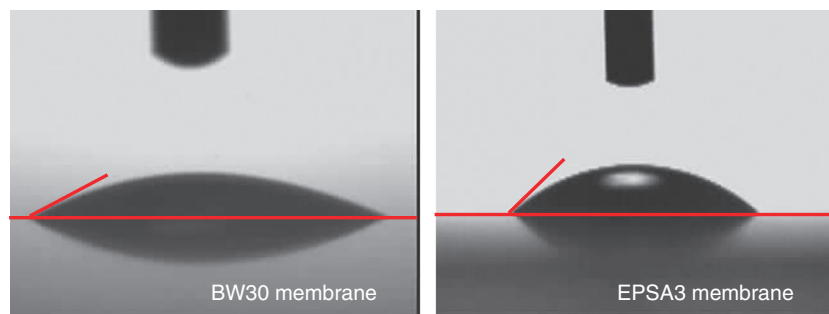

Figure 6 Contact-angle measurement for membranes BW30 and ESPA3. The PVA-coated membrane BW30 is much more hydrophilic than the uncoated membrane ESPA3. Unpublished photos.
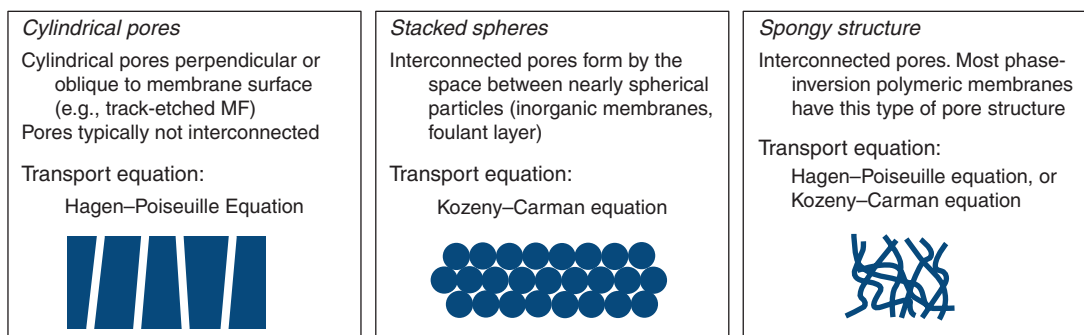

Figure 7 Types of membrane pore structures. Modified from Mulder M (1996) *Basic Principles of Membrane Technology*, 2nd edn. Dordrecht: Kluwer.

determined by the Hagen–Poiseuille equation:

$$L_p = \frac{\varepsilon r_p^2}{8\eta\tau l_m} \qquad (3)$$

where L_p is the water permeability of porous membranes, ε the membrane porosity, r_p the pore radius, η the viscosity of water, τ the tortuosity of the membrane, and l_m the thickness of the rejection layer. Another type of well-defined pore structure closely resembles stacked spheres (**Figure 7**), a structure typical for inorganic porous membranes prepared from spherical particles. Interconnected pores are formed by the space between the particles. The same pore structure can also be used to describe foulant cake layers formed by the deposition of colloids or suspended particles. Stacked-spheres pore structure can be modeled by the Kozeny–Carman equation:

$$L_p = \frac{\varepsilon^3}{K(1-\varepsilon)^2 S^2 \eta l_m} \qquad (4)$$

where K is the Kozeny–Carman coefficient and S the specific surface area of the particles. For perfect spherical particles, $S = 3/r_p$, $K = 5$, and $\varepsilon = 0.4$. Many other porous membranes have much more complicated pore structures. For example, polymeric membranes prepared via phase inversion may have a spongy structure. The pores tend to be highly interconnected with a high tortuosity and a wide size distribution. A log-normal pore-size distribution is sometimes assumed for modeling purpose (Aimar *et al.*, 1990). The Hagen–Poiseuille and/or Kozeny–Carman equation are widely used to approximate the transport properties of this type of membrane. The pore structural parameters of porous membranes prepared by different methods are summarized in **Table 5**.

4.11.3   Membrane Materials and Preparation

Polymers are the most popular materials used for membrane fabrication. Being membrane materials, the polymers should demonstrate thermal and chemical stabilities, good mechanical strength, and ability to form flat sheet or hollow fiber membranes easily. The two major techniques for membrane preparation include the phase-inversion process and interfacial polymerization, which are widely used for commercial membrane productions.

4.11.3.1   Polymeric Membrane Materials

Most of materials such as polymer, ceramic, metal, carbon, and glass can be used to make membranes. Among these, polymeric materials are the most popular ones used for membrane fabrication. Being membrane materials, the polymers should demonstrate thermal stability over a wide range of temperatures and chemical stability over a range of pH, and possess good mechanical strength. In addition, they can also be processed into flat sheet or hollow fiber membranes easily. Some commercial and representative polymeric membrane materials are introduced in **Table 6** (Ren and Wang, 2010).

Commercial UF/MF membranes can be made by various materials ranging from fully hydrophilic polymers, such as CA, to fully hydrophobic polymers, such as polypropylene (PP). PS, PES, polyacrylonitrile (PAN), and polyvinylidene fluoride (PVDF) are between the two extremes. A hydrophilic surface tends to resist attachment due to absorption by organics, but it has the disadvantage of being less robust compared with hydrophobic membranes. In order to reduce membrane fouling tendency, the hydrophobic polymers are modified through various approaches such as the use of additives as pore formers, or blending with a hydrophilic polymer, or posttreatment. **Figure 8** provides the relative hydrophilicity of commonly used polymeric materials. The pros and cons of different membranes made by different polymers are summarized in **Table 7** (Pearce, 2007).

4.11.3.2   Hollow Fiber Preparation

4.11.3.2.1   Mechanism of membrane formation

Hollow fiber membranes can be made either by a phase-inversion process or by a melt spinning plus stretching process (Mulder, 1996; Strathmann, 1990). Normally, UF membranes are produced by the phase inversion, which makes the membrane a precisely controlled asymmetric structure by varying the pore size over a wide range, while MF membranes can be fabricated by either process.
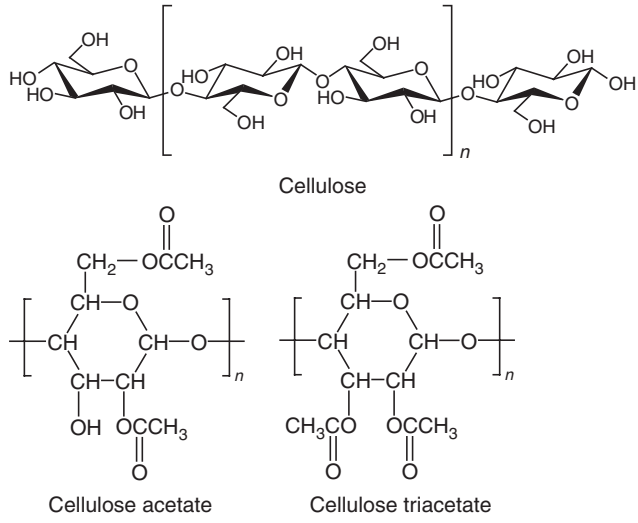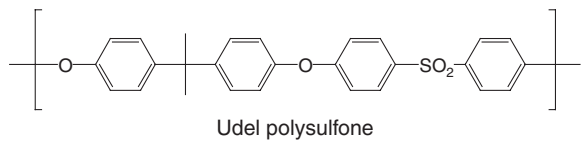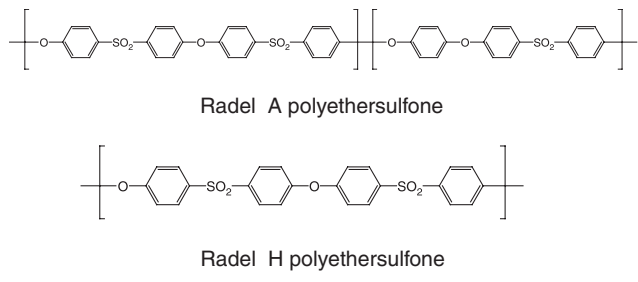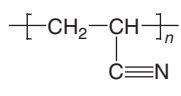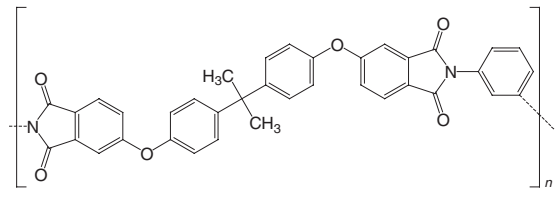
Phase inversion refers to the process by which a polymer solution (in which the solvent system is the continuous phase) inverts into a swollen three-dimensional macromolecular network or gel (where the polymer is the continuous phase) (Kesting, 1985). The essence of phase inversion is the appearance in a polymer solution of two interdispersed liquid phases (a polymer-rich phase and a solvent-rich phase) due to the change of the state of the polymer solution caused by the

Table 5   Pore structure of different types of porous membranes

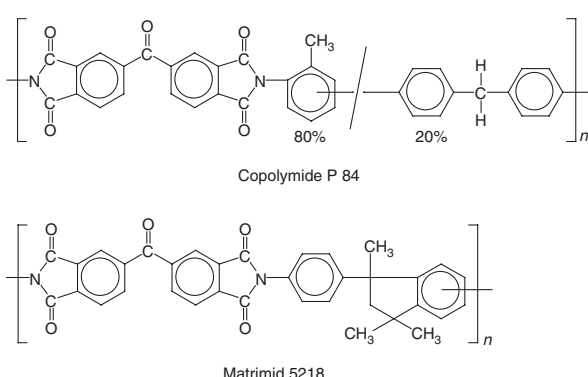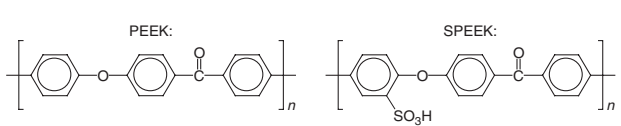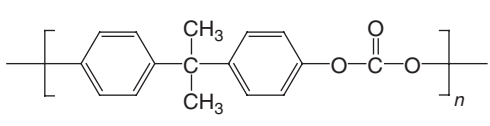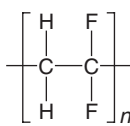| Pore structure	Pore size (μm)	Pore-size distribution	Porosity	Tortuosity	Symmetry	Fabrication method
Microfiltration						
Stacked spheres	0.1–20	Narrow	0.1–0.2	Low	Symmetrical	Sintering
Stretch pores	0.1–3	Wide	High, up to 0.9	Straight pores	Symmetrical	Stretching
Cylindrical pores	0.05–5	Nearly uniform	Low, up to ∼0.1	Straight pores	Symmetrical	Etching
Spongy structure	0.1–10	Wide, log-normal	0.3–0.7	Tortuous pores	Symmetrical/asymmetrical	Phase inversion
Ultrafiltration						
Spongy structure	0.001–0.1	Wide, log-normal	0.01–0.2	Tortuous pores	Asymmetrical	Phase inversion

Adapted from Mulder M (1996) *Basic Principles of Membrane Technology*, 2nd edn. Dordrecht: Kluwer.

Table 6   Commercial and representative polymeric membrane materials

Polymer	Structure	Properties
Cellulose and cellulose acetate (CA)	Cellulose Cellulose acetate Cellulose triacetate	• Cellulose is highly hydrophilic and crystalline. • Cellulose is mainly used for dialysis membrane preparation. • Cellulose acetate, diacetate, triacetate and their blends are widely used to make MF, UF, and RO membranes. • Cellulose and cellulose acetate membranes are susceptible to hydrolysis and microbial attack. • They are only stable over limited pH range between 4 and 6.5.
Polysulfone (PS)	Udel polysulfone	• PS is an amorphous polymer. • It belongs to the group of high-performance polymers with excellent chemical and thermal stability. • PS is mainly used to form UF, MF, and gas separation membranes. • PS is also used to form the porous support layer of many RO, NF, and some gas separation membranes.
Polyethersulfone (PES)	Radel A polyethersulfone Radel H polyethersulfone	• PES membranes have very high chemical and thermal stability. • Like PS material, PES membranes are affected by aromatic hydrocarbons or ketones. • PES membranes are slightly less • hydrophobic than PS membranes. • PES membranes are mainly used in UF, MF, and dialysis.
Polyacrylonitrile (PAN)		• PAN possesses superior resistance to hydrolysis and oxidation. • It is mainly used to prepare UF membranes and porous supports of composite membranes.
Polyetherimide (PEI)		• PEI is an amorphous thermoplastic with characteristics similar to the related plastic polyether ether ketones (PEEKs). • PEI cannot be used in contact with chloroform and dichloromethane. • It is a good material for the fabrication of the integrally asymmetric membranes for gas separation and pervaporation. • PEI is also used to fabricate the support of composite flat sheet membranes.

(*Continued*)

Table 6   Continued

Polymer	Structure	Properties
Polyamide (PA)	 Aliphatic polyamides (nylon *x* or nylone *x,y*)	• A PA is a polymer containing monomers of amides. • The basic aliphatic polyamides are referred as nylons which possess good thermal stability and mechanical strength, and are resistant to many organic solvents. • PA is used as the thin dense layer for RO and NF, but it has lower chlorine tolerance • The porous polyamide membranes have been commercialized for many years.
Polyimide (PI)	 Copolymide P 84 Matrimid 5218	• Polyimides exhibit excellent thermal and chemical stability because of their high glass transition temperature. • P84 is an amorphous commercial copolyimide with excellent resistance to many organic solvents. • Matrimide 5218 is another commercial polyimide. • Both polymers can be used as a material for making gas separation and NF membranes.
Polyether ether ketones (PEEKs)	PEEK: SPEEK: 	• PEEK has exceptional heat and chemical stability. • The high insolubility in common solvents makes PEEK membranes successfully being used in chemical processes as a solvent-resistant membrane. • The sulfonated PEEK (SPEEK) is soluble in common solvents, which can be used for the preparation of hydrophilic membranes or ion-exchange membranes.
Polycarbonate (PC)		• PC is a transparent thermoplastic with high-performance properties. • It is mainly used for track-etched membranes with well-defined pore structures and very good mechanical strength. • PC can also be used to make UF and MF membranes by the phase-inversion process.
Polyvinylidene fluoride (PVDF)		• PVDF is semi-crystalline with a very low glass transition temperature. • It is the most popular and available hydrophobic membrane material to be used for making MF by phase-inversion process. • It has excellent chemical resistance and thermal stability. • It is resistant to most inorganic and organic acids and tolerant to a wide pH range.

(Continued)

Table 6   Continued

Polymer	Structure	Properties
Polypropylene (PP)	$-[CH_2-CH]_n$ $\quad\quad CH_3$	• PP membrane is normally hydrophobic with high chemical stability. • Hydrophobic PP membrane is ideal for the filtration of aggressive solvents. • PP membranes are much cheaper than PTFE membranes.
Polytetrafluoroethyl-ene (PTFE)	$\left(\begin{matrix} F & F \\ C - C \\ F & F \end{matrix} \right)_n$	• PTFE is highly crystalline and demonstrates a very high resistance to chemical attack. • It cannot be formed by phase-inversion techniques. • PTFE membranes are formed by melt extrusion followed by stretch cracking. • The membranes are hydrophobic and need pre-wetting with a nonpolar solvent before use.

Adapted from Mulder M (1996) *Basic Principles of Membrane Technology,* 2nd edn. Dordrecht: Kluwer, and from Ren JZ and Wang R (2010) Preparation of polymeric membranes. In: Wang LK, Chen JP, Hung YT, and Shammas NK (eds.) *Handbook of Environmental Engineering*, vol. 13, ch. 2. Totowa: Humana Press.
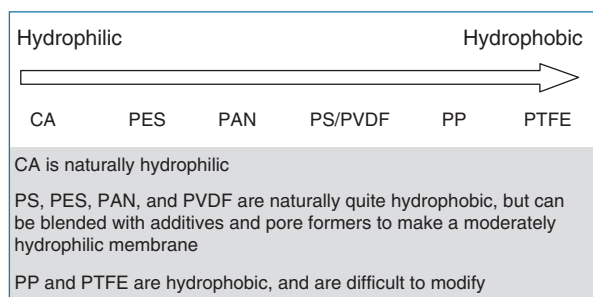
Hydrophilic					Hydrophobic
→ → → → → → → → → → → → → → → → →					
CA	PES	PAN	PS/PVDF	PP	PTFE

CA is naturally hydrophilic

PS, PES, PAN, and PVDF are naturally quite hydrophobic, but can be blended with additives and pore formers to make a moderately hydrophilic membrane

PP and PTFE are hydrophobic, and are difficult to modify

Figure 8   Relative hydrophilicity of commonly used polymeric materials. CA, cellulose acetate; PAN, polyacrylonitrile; PES, polyethersulfone; PS, polysulfone; PVDF, polyvinylidene fluoride; PP, polypropylene; PTFE, polytetrafluoroethylene. Modified from Pearce G (2007) Introduction to membranes: Membrane selection. *Filtration and Separation* 44: 35–37.

Table 7   Pros and cons of different membranes

Polymer	Properties
CA	Good permeability and rejection characteristics Susceptible to hydrolysis Limited pH resistance Chlorine tolerant and fouling resistant
PES, PVDF, PS, PAN	Ability to modify properties through polymer blend Good strength and permeability PVDF best for flexibility and use with air scour PES best for polymer blending and UF rating
PP	Susceptible to oxidation Limited blend capability

CA, cellulose acetate; PAN, polyacrylontrile; PES, polyethersulfone; PP, polypropylene; PS, polysulfone; PVDF, polyvinylidene fluoride.
Adapted from Pearce G (2007) Introduction to membranes: Membrane selection. *Filtration and Separation* 44: 35–37.

alteration of its surrounding environment or operating conditions, followed by crystallization, gelation, or vitrification. In other words, a liquid polymer solution is precipitated into two phases: (1) a polymer-rich phase that will form the matrix of the membrane; (2) a polymer-poor phase that will form the membrane pores in an unstable nascent membrane structure. The porous asymmetric membrane morphology is then fixed according to the subsequent solidification process.

There are different approaches to make the polymer solution precipitate, such as cooling, immersion in a nonsolvent coagulant bath, evaporation, and vapor adsorption. Depending on the change of the operating parameters that induce the phase inversion, two different separation mechanisms are involved:

• *Thermally induced phase separation (TIPS).* The precipitation is achieved by decreasing the temperature of the polymer solution. This process can be used for PVDF membrane preparation.
• *Diffusion-induced phase separation (DIPS).* Diffusional mass exchange, because of the contact of the polymer solution with a nonsolvent, leads to a change in the local composition of the polymer film and then precipitation is induced. CA, PS, PES, PVDF, and PAN membranes are made by this method.

TIPS. It is one of the main approaches for the preparation of microporous membranes. In the TIPS process, a polymer is dissolved into a solvent or a mixture of solvent and nonsolvent, and a homogeneous solution is formed only at elevated temperature. By cooling down the homogeneous

solution, the phase separation is induced. Once the polymer-rich phase is solidified, the porous membrane structure can be created by removing the solvent via extraction. Membrane formation by TIPS can be illustrated by the phase diagram of a polymer solution as a function of temperature from the basic point of thermodynamics, as shown in **Figure 9**.

From the phase diagram, it can be seen that there exists three different phase areas of homogeneous solution phase I, the liquid–liquid demixing (metastable areas II, III, and unstable area IV) and one crystalline phase V, which are separated by a binodal curve, a spinodal curve, and a crystallization curve. If a homogeneous polymer–solvent mixture at a temperature T_A, as indicated by point A in **Figure 9**, is cooled to the point M, the solution separates spontaneously into two phases after it crosses the spinodal curve. Upon further cooling to the temperature T_{gel}, as indicated by point B, the composition of the polymer-rich phase reaches point B″, and the point B′ represents the solvent-rich, the polymer-lean

liquid phase. At this moment, the polymer-rich phase starts to solidify and forms the solid membrane structure, and the polymer-lean phase forms the pores. An interpenetrating three-dimensional network can be obtained.

DIPS. The invention of the first integral asymmetric membranes by DIPS was a major breakthrough in the history of RO and UF membrane development (Loeb and Sourirajan, 1964; Kesting, 1985). DIPS can be realized through immersing the casting solution in a nonsolvent coagulant bath, evaporating the solution and using vapor adsorption. **Figure 10** illustrates the concepts of three DIPS processes.

For an immersion precipitation process, at least three components of polymer, solvent, and nonsolvent are involved. The membrane formation can also be illustrated with a ternary phase diagram as shown in **Figure 11**. In the diagram, four different regions are shown: one solution phase (region I), liquid–liquid two phases (region II), liquid–solid two phases (region III), and one solid phase (region IV).
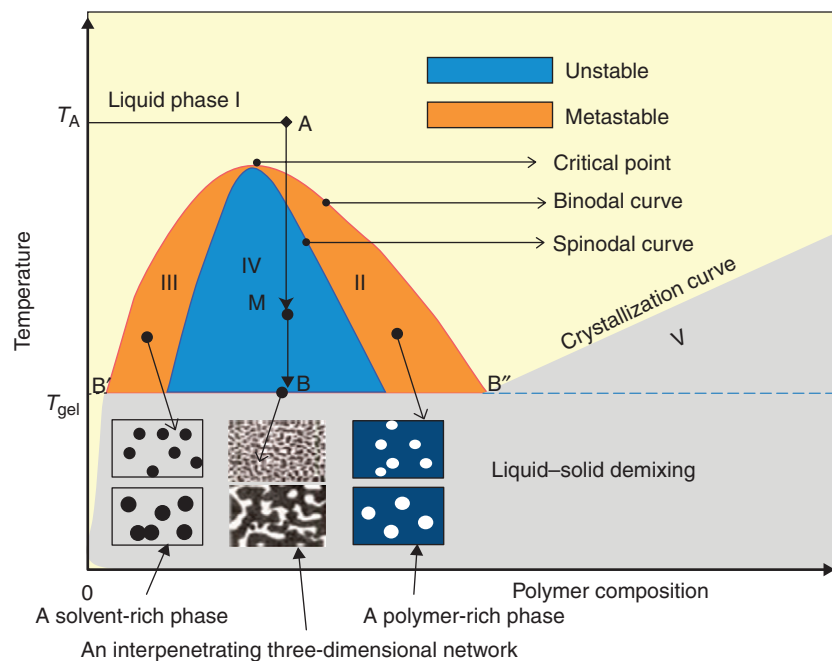
Figure 9   Schematic phase diagram of thermally induced phase separation. Modified from van de Witte P, Dijkstra PJ, van de Berg JWA, and Feijen J (1996) Phase separation process in polymer solutions in relation to membrane formation. *Journal of Membrane Science* 117: 1–31.
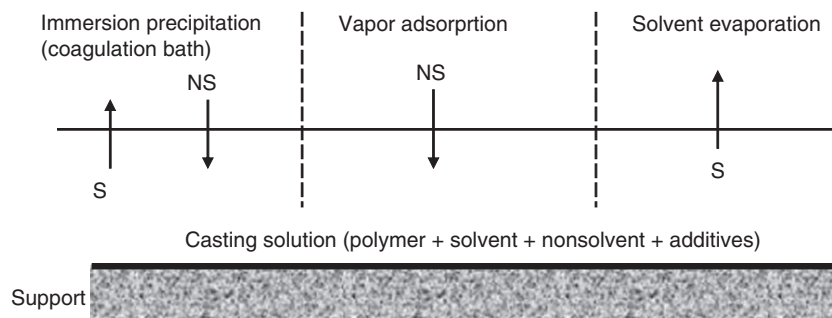
Figure 10   Representation of three DIPS processes (S: solvent; NS: nonsolvent). Modified from Ren JZ and Wang R (2010) Preparation of polymeric membranes. In: Wang LK, Chen JP, Hung YT, and Shammas NK (eds.) *Handbook of Environmental Engineering*, vol. 13, ch. 2. Totowa, NJ: Humana Press.

Figure 11 Schematic diagram of membrane formation process for DIPS. Modified from Ren JZ and Wang R (2010) Preparation of polymeric membranes. In: Wang LK, Chen JP, Hung YT, and Shammas NK (eds.) *Handbook of Environmental Engineering*, vol. 13, ch. 2. Totowa, NJ: Humana Press.

Figure 12 Schematic diagram of a hollow fiber spinning line.

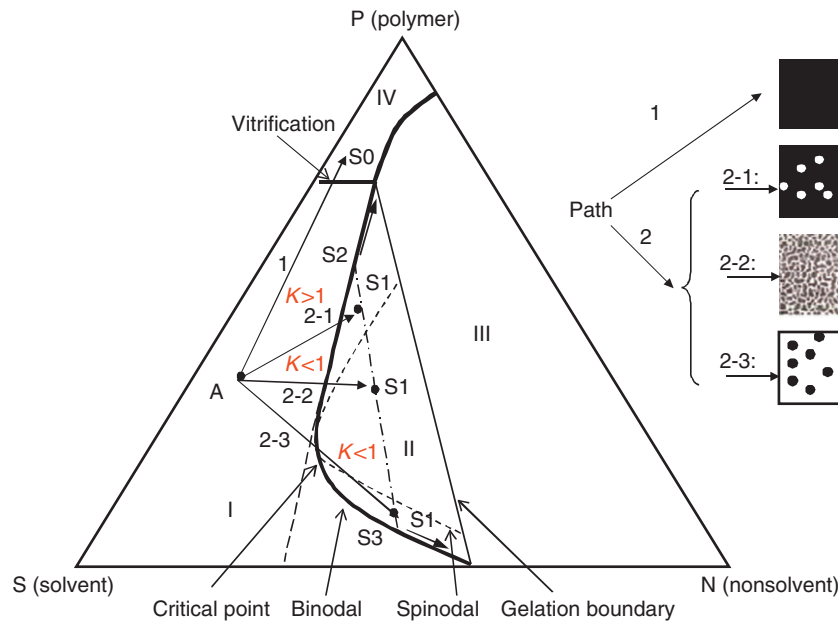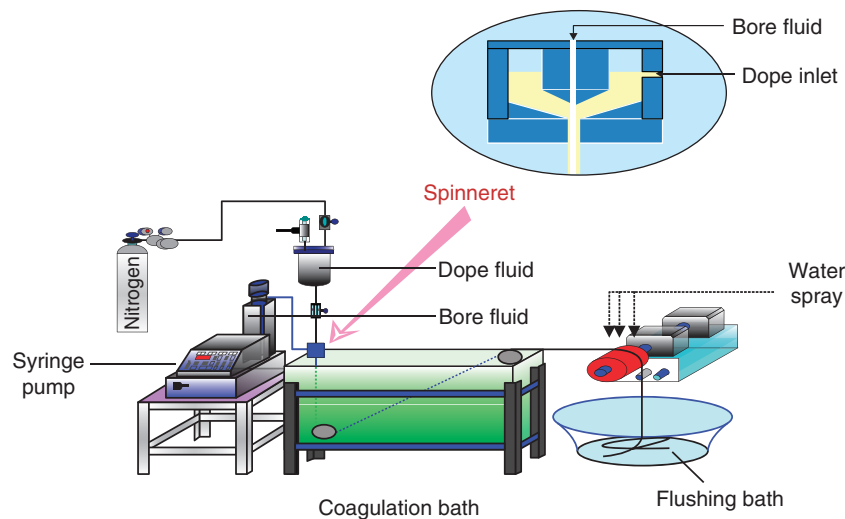Point A represents the initial composition of a casting solution. If the polymer solution is immersed into a nonsolvent bath, there are two possible composition paths, 1 and 2 (2-1, 2-2, 2-3). For path 1, the polymer solution undergoes a glass transition and goes into the solid phase IV directly. Consequently, the solution becomes a homogeneous glassy film. For the path 2, gelation dominates the formation of the porous membrane morphologies. When the composition path crosses the binodal curve and reaches point S1, liquid–liquid phase separation (S1 → S2 + S3) occurs. The polymer-rich phase is represented by point S2 and polymer lean phase is represented by point S3. Depending on the location of point S1, three different nascent membrane morphologies are formed by (a) the nucleation and growth of the polymer-poor phase (path 2-

1), which leads to a morphology with dispersed pores; (b) the spinodal decomposition (path 2-2), which leads to a bi-continuous network of the polymer-poor and polymer-rich phases without any nucleation and growth due to instantaneous demixing; and (c) the nucleation and growth of the polymer-rich phase (path 2-3), which leads to low-integrity powdery agglomerates. Such membrane morphology is not practical and thus it rarely happens in membrane formation.

4.11.3.2.2 Fabrication of hollow fiber membranes
Polymeric hollow membranes were first introduced in 1966 (Mahon, 1966). A schematic diagram of a hollow fiber spinning line is shown in Figure 12. Hollow fiber membranes can

be fabricated by either wet or dry-jet wet spinning process, where an air gap between the spinneret and the coagulation bath can be zero or a certain value. Basically, the polymer dope container is connected to a N_2 gas cylinder or a pump. The dope is dispensed under pressure or pumped through a spinneret at a controlled rate, and goes through an air gap before immersing into a coagulation bath. Water is (typically) used as external coagulant, while a mixture of milli-Q Water and a solvent with varying ratios is used as the bore fluid. The nascent hollow fiber is taken up by a roller at a free falling or controlled velocity and stored in a water bath to remove

residual solvent for further characterization (Strathmann, 1990; Shi et al., 2008). Figure 13 shows the morphology of poly(vinylidene fluoride-co-hexafluoropropylene) (PVDF-HFP) asymmetric microporous hollow fiber membranes made by the DIPS process (Shi et al., 2008).

Being an extremely complex process, the fabrication of hollow fiber membranes requires highly sophisticated mechanical, thermodynamic, and kinetic considerations. The spinning parameters involved are summarized in Figure 14. Mckelvey et al. (1997) have provided detailed guidance on how to control macroscopic properties of hollow fiber
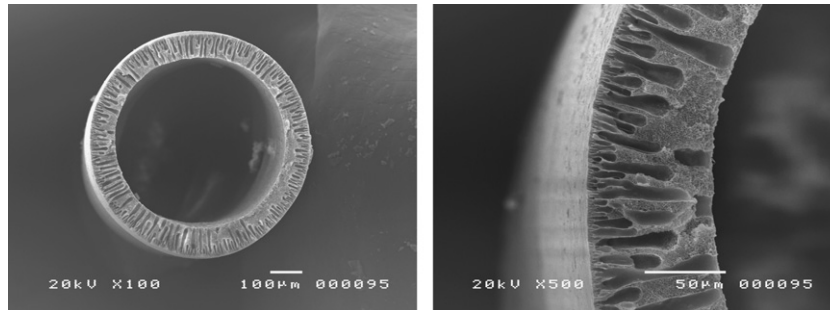
Figure 13 Cross-section morphology of the hollow fibers spun from the PVDF-HFP/NMP dopes without an additive. Reproduced from Shi L, Wang R, Cao YM, Liang DT, and Tay JH (2008) Effect of additives on the fabrication of poly(vinylidene fluoride-co-hexafluoropropylene) (PVDF-HFP) asymmetric microporous hollow fiber membranes. *Journal of Membrane Science* 315: 195–204, with permission from Elsevier.
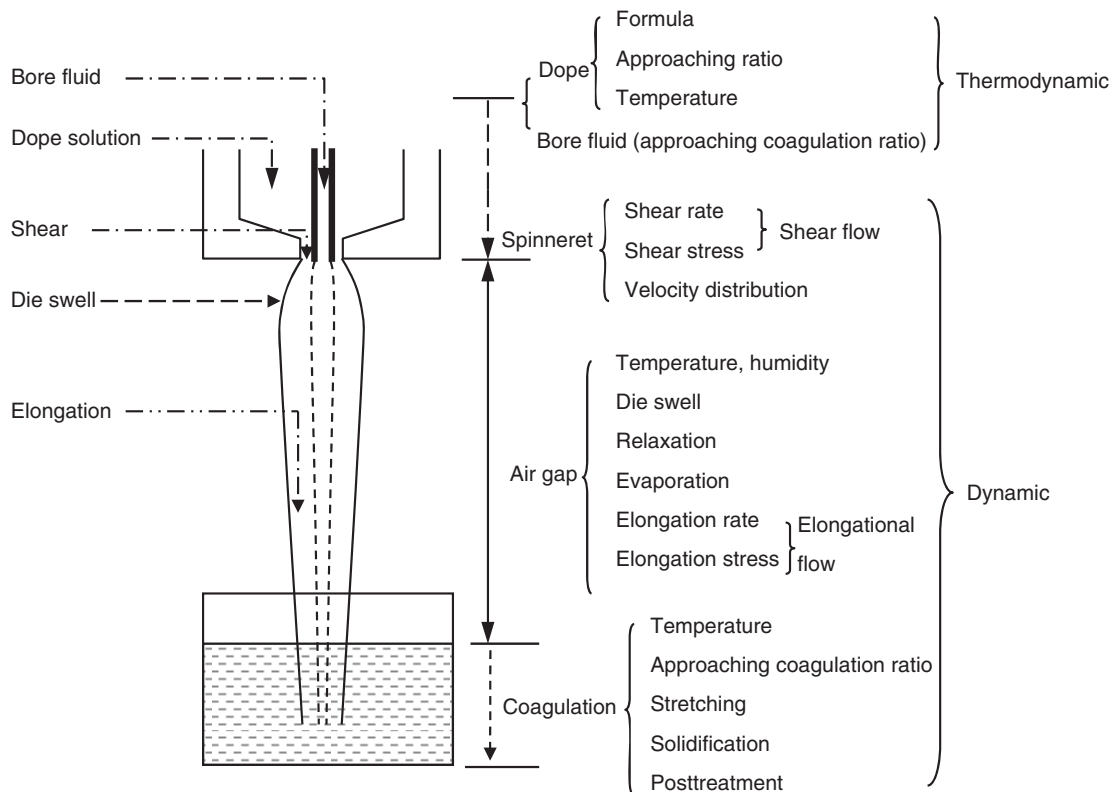
Figure 14 Parameters involved in a dry-jet wet spinning process for hollow fiber membranes. Modified from Ren JZ and Wang R (2010) Preparation of polymeric membranes. In: Wang LK, Chen JP, Hung YT, and Shammas NK (eds.) *Handbook of Environmental Engineering*, vol. 13, ch. 2. Totowa, NJ: Humana Press.

membranes using dominant process parameters, including spinneret design, dope extrusion rate, air gap distance, bore fluid extrusion rate, solvent concentration in the bore fluid, vitrification kinetics, etc., and how to determine the optimal macroscopic properties. The effect of shear rate on the performance and morphology of hollow fiber membranes can also be found in the literature (Qin et al., 2001).

4.11.3.3 TFC Membrane Preparation

In addition to the integral asymmetric membranes, which are produced by the phase-inversion process, composite membranes are also widely used in industry. For instance, many NF and RO membranes are formed with a composite structure (see also Section 4.11.2). A typical composite membrane is shown schematically in Figure 4. Normally, composite membranes are made in a two-step process: (1) fabricating a microporous support and (2) depositing/casting a barrier layer on the surface of the microporous support layer. This approach provides great flexibility for selecting different materials to tailor the membrane structure and properties.

Today, the most important technique for manufacturing composite membranes is the interfacial polymerization of reactive monomers on the surface of a microporous support membrane. This technique was developed in the mid-1970s (Cadotte, 1977). A PS microporous membrane is soaked in an aqueous solution containing 0.5–1% polyethyleneimine, and then brought in to contact with a 0.2–1% solution of toluene diisocyanate in hexane. These two reagents react rapidly on the membrane surface, forming the selective layer of the composite membrane. A heat curing step leads to further crosslinking of the polyethyleneimine, which extends into the pores of the support membrane (Strathmann, 1990). More information on TFC membrane properties is given in Section 4.11.2.2.

4.11.3.4 Ceramic Membrane Preparation

Similarly to polymeric membranes, ceramic membranes have been developed for many process applications, including MF and UF in the water industry. They are more thermally and chemically stable than polymer membranes with much greater mechanical strength and higher structural stability, which allows ceramic membranes to be used in harsh environments.

Generally, the structure of ceramic membranes is asymmetric, consisting of a macroporous support, one or two mesoporous intermediate layers, and a microporous (or a dense) top layer. The support layer provides mechanical strength, the middle layers bridge the pore-size differences between the support and the top layers, and the thin top layer determines the separation. The preparation of a ceramic membrane support normally involves the following steps: (1) forming particle suspensions; (2) packing the particles in the suspensions into a membrane precursor with a certain shape using various shaping techniques such as slip casting, tape casting, extrusion, and pressing; and (3) sintering the membrane precursor at elevated temperature (Li, 2007). The separation layers of composite ceramic membranes are made of SiO_2, Al_2O_3, ZrO_2, and TiO_2 materials, which can be formed on a membrane support via dip-coating, sol–gel, chemical vapor deposition (CVD), or electrochemical vapor deposition (EVD), followed by repeated firing steps. A detailed description of ceramic membrane preparation methods can be found in Li (2007).

The phase-inversion method which is commonly employed to spin polymeric hollow fiber membranes can also be used to prepare inorganic hollow fibers in combination with sintering step. The protocol of preparation is depicted in Figure 15. Basically, a desired spinning dope (a mixture of ceramic powder and polymer solution) is formed and passed through a spinneret to enter a water bath for precipitation. After posttreatment, the hollow fiber precursors are heated in a furnace to remove the organic polymer binder, and then calcined at a high temperature to allow the fusion and bonding to occur. Figure 16 shows the morphology of Zirconia hollow fibers membranes made by this method (Liu et al., 2006). Various factors such as the sintering temperature and the ratio of the selected ceramic powders to the polymer binders will affect the structure and performance of the resultant membranes.

4.11.4 Membrane Characterization

Membrane characterization is critical to the understanding of the chemistry and structure of membranes and to the identification of causes of membrane failures. This section also briefly reviews a wide range of commonly used characterization techniques, including pore-structure characterization, microscopic methods, as well as spectroscopic methods for information on membrane chemistry.

Membrane characterization is the basis for establishing the chemistry–structure–properties relationship that is a critical aspect in any new membrane development process. This can guide subsequent membrane optimization to achieve excellent separation efficiency and fouling resistance. Characterizing and understanding membrane chemistry and properties is also the key for selecting suitable membranes for a given application. A wide range of characterization methods have been applied to membrane characterization. This section briefly summarizes some of the most commonly used techniques (Table 8):

Performance tests. This involves measurements of membrane permeability and rejection of various solutes using a filtration setup. The performance data (e.g., rejection of probe molecules such as dextran or polyethylene glycol) can be used to determine pore-size distribution of a membrane (Aimar et al., 1990; Schafer et al., 2005).

Membrane porometry. Various porometry methods have been used to determine the pore-size distribution of MF and UF membranes. The bubble point method, which measures the pressure at which air bubbles start to pass through a wetted MF membrane, can be used to characterize pores $> 0.15\,\mu m$. Another method commonly used for MF membrane pore characterization is the mercury intrusion method, which is suitable for pores ranging from 3.5 to 1000 nm. Other methods include gas adsorption, permporometry, and thermoporometry, which are suitable for characterizing smaller pores. A comprehensive review of these methods can be found in Nakao (1994).
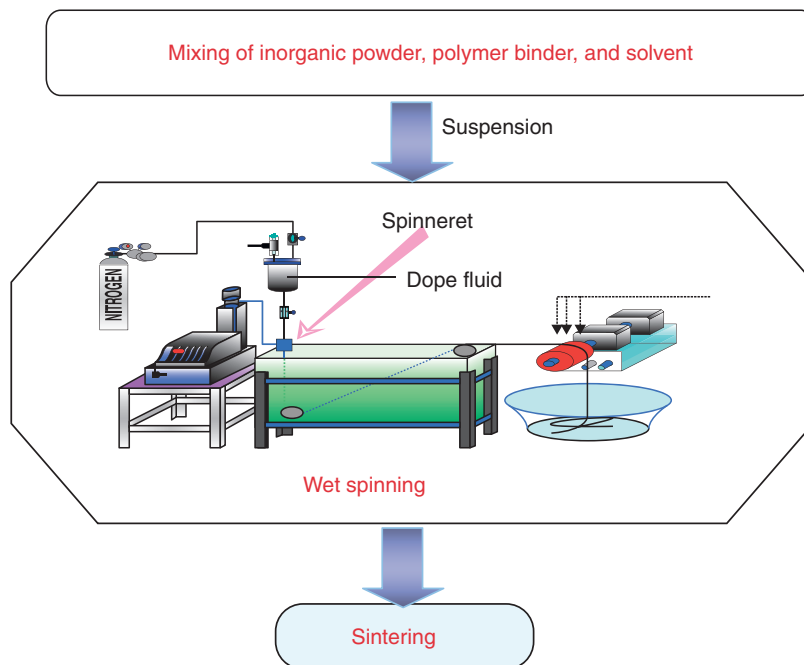
Figure 15 Protocol of preparing inorganic hollow fibers using modified phase-inversion method.
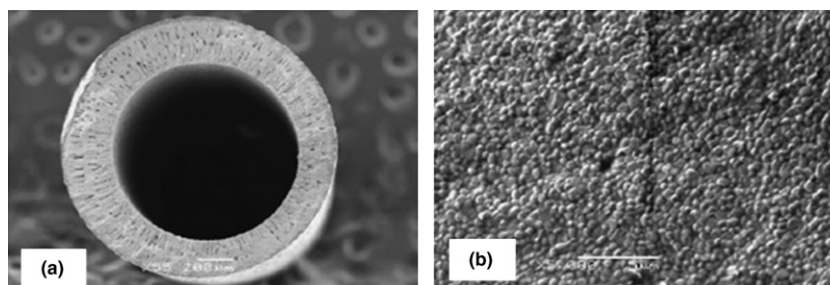

Figure 16 Morphology of zirconia hollow fiber membranes: (a) cross section and (b) outer surface Reproduced from Liu LH, Gao SJ, Yu YH, Wang R, Liang DT, and Liu M (2006) Bio-ceramic hollow fiber membranes for immunoisolation and gene delivery. I: Membrane development. *Journal of Membrane Science* 280: 762–770, with permission from Elsevier.

Microscopic methods. Microscopic methods are useful for the visualization of membrane morphology and structure. They can be used to study the surface features of a membrane as well as its cross section. Microscopic methods are also widely used for membrane pore-size characterization (Kim *et al.*, 1990). Where a foulant cake layer is present, microscopic investigation can provide great details about the morphology, structure, and properties of the layer. Conventional visible light microscopy is routinely used for membrane visualization due to its low cost and easy operation. However, its resolution is usually limited due to the relatively large wavelength of visible light. In contrast, electron microscopic methods, such as scanning electron microscopy (SEM) and transmission electron microscopy (TEM), offer much better resolution. SEM has been widely used to characterize the surface and cross section of both clean and fouled membranes at a resolution as good as 5 nm for polymeric samples. Where ultrathin (<100 nm in thickness) sections can be prepared, TEM can

provide a large amount of detail on the structural information of membranes and foulants (Tang *et al.*, 2007a; Freger, *et al.*, 2005). Other commonly used microscopic methods include atomic force microscopy (AFM) and confocal laser scanning microscopy (CLSM). AFM can provide valuable information on the surface features of a membrane, and it has become the standard method for characterizing membrane roughness. On the other hand, CLSM is a powerful method for biofilm characterization.

Spectroscopic methods. Spectroscopic methods provide essential information on the structure and chemistry of a membrane. For example, Fourier transform infrared spectroscopy (FTIR) is able to identify various chemical bonds in a membrane based on its adsorption of infrared irradiation (Tang *et al.*, 2007a). Both X-ray photoelectron spectroscopy (XPS) and energy dispersive spectroscopy (EDX) are widely used for identifying elements present in membranes. XPS is a highly surface-sensitive technique, with the ability to measure

Table 8 Commonly used membrane characterization methods

Type	Instrument	Information
Performance test	Membrane filtration setup	Permeability, rejection, and pore-size distribution inferred from transport models
Membrane porometry	Bubble point, mercury intrusion, gas adsorption, permporometry, thermoporometry	Information on membrane pore structure
Microscopic methods	SEM TEM AFM CLSM	Surface/cross-section features Cross section of membrane/foulant Roughness, surface morphology Foulant structure/composition
Spectroscopic methods	FTIR XPS EDX EIS	Membrane/foulant functional groups Elements/chemical binding Elemental mapping of foulants Structural information of sublayers
Other methods	Goniometer Streaming potential AFM force measurement	Hydrophobicity Surface charge Interaction force

AFM, atomic force microscopy; CLSM, confocal laser scanning microscopy; EDX, energy dispersive spectroscopy; EIS, electrical impedance spectroscopy; FTIR, Fourier transform infrared spectroscopy; SEM, scanning electron microscopy; TEM, transmission electron microscopy; XPS, X-ray photoelectron spectroscopy.

elemental composition and chemical binding information for the top 1–5 nm depth of the surface region (Tang *et al.*, 2007a). The technique is able to detect all elements except hydrogen with detection limits around 0.01 monolayer or 0.1% of the total elemental concentration. Compared to XPS, EDX is less sensitive. Nevertheless, EDX offers a unique advantage as it can be coupled to an SEM or TEM, which allows it to analyze microscale features at specific locations and to construct elemental mapping. EDX has been widely used in membrane autopsy to analyze chemical compositions of membrane foulants (Khedr, 2003). Recently, electrical impedance spectroscopy (EIS) has been used to characterize the layered structures of TFC-RO and NF membranes. This method is able to provide structural information (e.g., thickness and electrical properties) of each sublayer of a composite membrane (Coster *et al.*, 1996).

Other surface characterization techniques. Goniometer and streaming potential analyzer are widely used to characterize membrane surface hydrophobicity (via contact-angle measurements) and surface charge (via zeta potential measurements), respectively (Tang *et al.*, 2009a). AFM interaction force measurement is an emergent technique for membrane surface and foulant layer characterization (Bowen *et al.*, 1999; Lee and Elimelech, 2006; Tang *et al.*, 2009c). Using a colloidal cantilever probe with well-defined surface chemistry and calibrated spring constant, the AFM force measurement technique can be used to measure tiny interaction forces (~ 1 nN) between a membrane surface (either clean or fouled) and the probe. Such interaction forces correlate well with membrane fouling behavior (Tang *et al.*, 2009 c; Lee and Elimelech, 2006).

4.11.5 Membrane Modules

The membranes described in Sections 4.11.2 and 4.11.3 are produced as hollow fibers, tubes, and flat sheets. To use these membranes in large-scale processes, it is necessary to incorporate them into a membrane module. Important features of modules include packing density, ease of cleaning, and flow distribution. Several module geometries have been developed suited to the range of membranes and their applications in the water industry.

4.11.5.1 The Role of the Module

The membrane module, or element, has two major roles: (1) supporting the membrane and (2) providing efficient fluid management. Membranes are typically produced as flat sheets, tubes, or hollow fibers. The flat sheet and tubular forms are not self-supporting and the membranes must be placed on a porous support able to withstand the applied pressure and also facilitate permeate removal. Hollow fibers can be self-supporting, and operate outside-to-in or inside-to-out. The latter is also called lumen feed, where the lumen is the bore of the hollow fiber.

Good fluid management is vital for efficient membrane processing. The hydrodynamic conditions in the boundary layer at the membrane surface control the concentration polarization (CP) (see Section 4.11.6.3), which directly influences membrane performance. The various module designs deal with feed-side flow in different ways, attempting to balance boundary-layer mass transfer and the feed channel pressure losses. Fluid management also pertains to the downstream, permeate side of the membrane, because resistance to flow determines the downstream pressure losses and the net transmembrane pressures (TMPs). Several characteristics are potentially important in module design and are summarized in Table 9. In what follows, the various modules are described (Section 4.11.5.2), and their characteristics are summarized in Table 10.

4.11.5.2 Module Types

This section describes the most common modules used in the water industry. One early approach, not described, was the

plate-and-frame module which used stacks of flat sheet membranes on porous supports separated by flow channel spacers. Limitations due to packing density, pressure containment, and labor-intensive membrane replacement lead to the development of the SWM (see below).

4.11.5.2.1 Spiral-wound module

The SWM is the predominant design for RO and NF applied to the water industry (see Section 4.11.1.3 for some of the historical developments); as such, it is the workhorse for SWRO and water reclamation plant. The SWM uses flat sheet membranes sealed by gluing on three sides to form leaves attached to a permeate channel (tube) along the unsealed edge of the leaf. Inside each leaf is a permeate spacer which is a porous matrix designed to support the membrane without compression, and to have a high hydraulic conductivity for permeate flow to the permeate tube (see Figure 17(a)). A net-like feed channel spacer fits between the leaves and defines the channel height (typically $\sim 1\,mm$). Several leaves are fixed to and then wound around the permeate tube and given an outer rigid casing (Figures 17(b) and 17(c)). The module has an anti-telescoping end cap which provides support to counter axial pressure drops. It should be emphasized that the feed channel spacer plays an important role as it enhances the effect of crossflow and promotes boundary layer mass transfer that controls CP (see Section 4.11.6.3). Table 12 (Section 4.11.6) provides information about the mass transfer correlations for different spacer geometries.

The SWM comes in a standard diameter of 8 in (203 mm), but 2.5 and 4 in are also used for pilot or small scale, and 16 in SWMs are being introduced. The SWM is fitted into standard pressure vessels which can take several elements connected in series with O-ring seals to prevent bypassing and feed-to-permeate flow. Up to eight modules could be present in a pressure vessel, and many vessels are connected in an array (examples given in Section 4.11.7.2). A large desalination plant could have 20 000–50 000 modules.

4.11.5.2.2 Tubular module

Tubular modules have the membrane surface on the inside of the tubes. They have several niche applications at the medium scale. Diameters are in the range 5–25 mm. The modules are similar to the shell and tube heat exchanger (Figure 18) with tubes connected in parallel and series. Some designs have the membrane tubes inserted into porous metal support tubes, and are able to withstand pressure for RO and NF. In other cases, the tubes are self-supporting and the burst pressure of the tubes limits it to UF/MF applications. Tubular modules are also produced in ceramic materials as multichannel monoliths with UF or MF capability; there are reported applications in water treatment. For RO and NF tubular modules are operated with crossflow in the turbulent flow regime which provides good control of CP, but at a relatively high energy cost. This type of module is suitable for feeds with high turbidity. An interesting example is remote-area water treatment which uses tubular NF with automatic foam ball cleaning for chemical-free water treatment of colored waters (see reference 12 in Fane (2005)).

4.11.5.2.3 Hollow fiber module (contained)

Hollow fiber membranes are self-supporting, that is, the walls can be strong enough to avoid collapse or bursting. Outer diameters are in the range of 0.5–1.0 mm with inner lumen diameters of <0.3 to 0.8 mm. Hollow fiber modules (HFMs) are either contained (filtration under pressure) or submerged (filtration under suction); Section 4.11.5.2.4 deals with submerged modules. Contained HFMs involve thousands of fibers arranged in a bundle and potted by epoxy in an outer shell (Figure 19). The design is similar to the shell and tube design for tubular membranes, but can be operated with feed in the shell side (out-to-in) or feed in the lumen (in-to-out), depending on the membranes and the application. HFMs with shell-side feed are externally pressurized and some RO hollow

Table 9   Module characteristics of importance

Characteristic	Significant influence on
Packing density	System size, footprint, and (probably) cost
Energy use	Costs $= f$\{operating pressure, flow rate, flow resistance, flow regime\}
Fluid management	Concentration polarization, flux/pressure relationship, fouling, and cleaning
Standardization	Flexibility in terms of choice of membrane supplier
Replacement	Maintenance and labor costs
Cleaning	System availability, downtime, and time-averaged production

Table 10   Characteristics of different module concepts

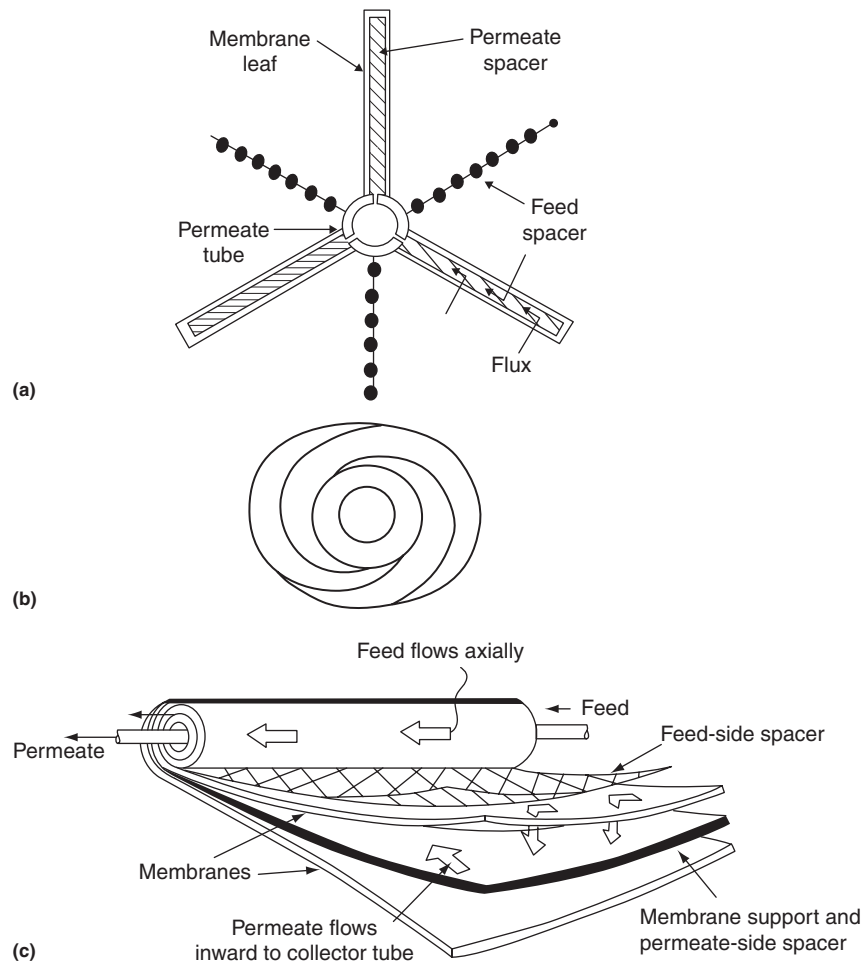| Characteristic	Spiral wound	Tubular	Hollow fiber	Submerged
Packing density ($m^2\,m^{-3}$)	High (500–1000)	Low–moderate (70–400)	High (500–5000)	Moderate
Energy use	Moderate (spacer losses)	High (turbulent)	Low (Laminar)	Low
Fluid/fouling management	Good (no solids) Poor (solids)	Good	Moderate (in-to-out) Poor (out-to-in)	Moderate
Standardization	Yes	No	No	No
Replacement	Element	Tubes (or element)	Element	Element (or bundle)
Cleaning	Can be difficult (solids)	Good – physical cleaning possible	Backflush (MF/UF)	Backflush (HF) (MF/UF)

Figure 17 (a) Spiral-wound module showing membrane leaves and spacers. (b) Spiral-wound module with leaves wrapped around permeate tube. (c) Spiral-wound module showing flow paths. (a–c) Reproduced from Fane AG (2005) Module design and operation. In: Schaefer AI, Fane AG, and Waite TD (eds.) *Nanofiltration – Principles and Applications*, pp. 67–88. Oxford: Elsevier, with permission from Elsevier.
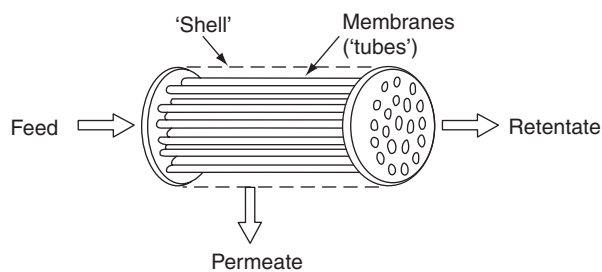
Figure 18 Tubular module (shell-and-tube arrangement). Reproduced from Fane AG (2005) Module design and operation. In: Schaefer AI, Fane AG, and Waite TD (eds.) *Nanofiltration – Principles and Applications*, pp. 67–88. Oxford: Elsevier, with permission from Elsevier.

fibers can withstand high pressures up to the level of SWRO. In some special cases, seawater applications with hollow fibers of cellulose triacetate are used (Kumano and Fujiwara, 2008); their major advantage is the ability to withstand chlorine to control biofouling. However, in the vast majority of seawater RO desalination plants the HFM has been superseded by the SWM.

HFMs with shell-side feed are commonly used in low-pressure membrane applications (UF and MF), such as water treatment and pretreatment (see Table 2). These applications often use dead-end operation (see Section 4.11.7.1) with intermittent backwash from the lumen to the shell. Compared with submerged HFMs, the contained modules have a wider range of TMPs available. HFMs with lumen-side feed are also used for water treatment and pretreatment. Operation is either with crossflow or with dead-end flow, depending on the solids content (low solid favors use of dead-end with backwash). Intermittent two-phase (air–liquid) flow is often applied to HFMs during the backwash cycle. Continuous two-phase flow may be implemented in cases where the HFM (lumen-side feed) is used with high solids, such as MBRs (see Section 4.11.1.2.4).

4.11.5.2.4 Submerged module
Submerged (or immersed) modules involve membranes positioned in a flooded tank at atmospheric pressure typically open at the top. The liquid to be filtered is fed to the tank and permeate is removed from the module under suction, either

Figure 19   Contained hollow fiber module. Reproduced from Fane AG (2005) Module design and operation. In: Schaefer AI, Fane AG, and Waite TD (eds.) *Nanofiltration – Principles and Applications*, pp. 67–88. Oxford: Elsevier, with permission from Elsevier.
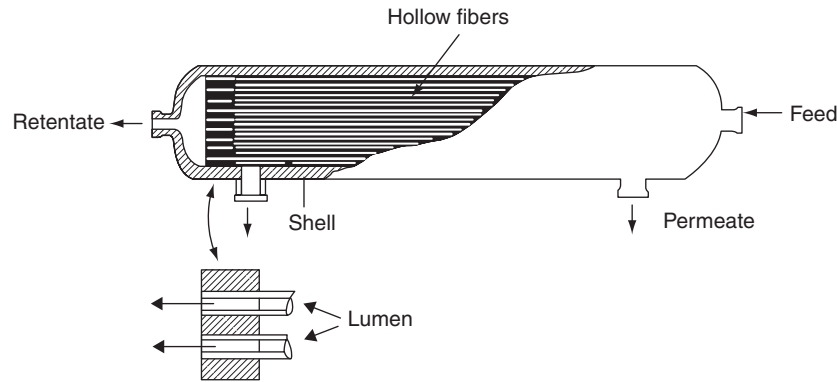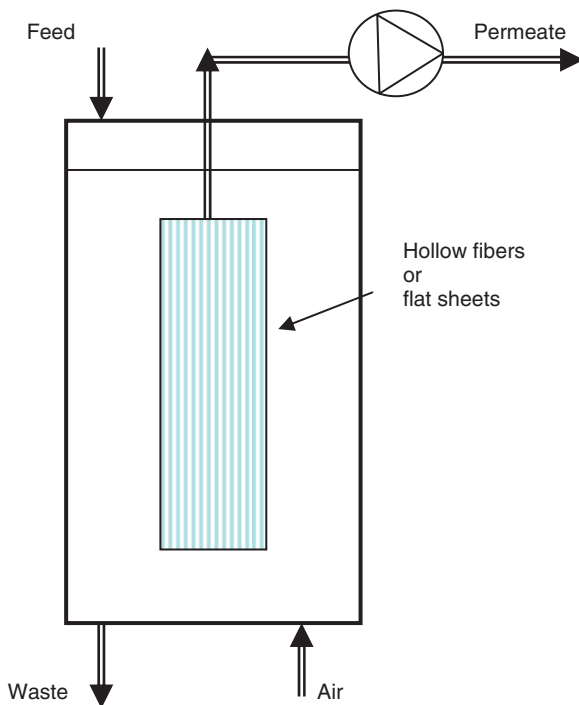

Figure 20   Submerged membrane module.

by a pump or by gravity. The concentrate is removed continuously or intermittently from the tank. **Figure 20** depicts the general features of a submerged membrane system, which include:

1. an open tank (no pressure vessel),
2. modules in bundles of fibers or vertically aligned flat plates,
3. permeate removed by suction, and
4. TMPs <1 atm.

Submerged modules use low-pressure MF and UF membranes; they are unsuitable for NF or RO due to the limited TMP. For low solid feeds, such as water treatment or pretreatment to RO, submerged hollow fibers are commonly used. Operation is usually dead-end cycles with regular backwash and

intermittent air scour. Flat sheets are not used in these applications because they cannot be backwashed. In these low solid operations both submerged and contained HFMs appear to be equally popular. In some cases, submerged HFMs may offer marginal cost advantages, but they have less turn-up/turn-down capability and are heavier than contained HFMs.

For high solid content feeds, such as MBRs, submerged modules are either hollow fibers or flat sheets, with continuous or rapidly intermittent air scour, and occasional backwash (hollow fibers). Submerged modules are more popular than contained modules for MBRs. There is no standardization in submerged membranes and there are many commercial suppliers; for example, Judd (2006) describes 12 different MBRs using submerged membranes. A more detailed account of submerged membranes can be found elsewhere (Fane, 2008).

4.11.6   Basic Relationships and Performance

Membrane performance (such as flux and rejection) is determined by the mass transport inside a membrane as well as the transport toward the membrane surface. The mass transport inside a membrane defines the basic relationship between flux and the driving force. In addition, it determines the intrinsic retention properties of the membrane. Due to its retentive nature, solutes transported toward a membrane will tend to accumulate near the membrane surface, leading to a higher solute concentration near the surface compared to the bulk concentration. This phenomenon is known as CP. Another important phenomenon in pressure-driven membrane processes is membrane fouling, that is, the deposition of contaminants on a membrane surface and/or inside membrane pores. Both CP and fouling can adversely affect membrane flux and rejection. Thus, they need to be carefully controlled in membrane operation.

4.11.6.1   Membrane Flux and Rejection

Flux and rejection are among the most important performance parameters for any membrane process. Membrane flux of a given species can be defined as the mass (or volume) of that species passing through a unit membrane area within a given duration. For applications in water and wastewater treatment,

the water flux is of particular interest, as this directly relates to the membrane productivity and thus process economics (refer to Section 4.11.7 for more details). Water flux J_w is typically defined as

$$J_w = \frac{Q_p}{A_m} \qquad (5)$$

where Q_p is the volumetric flow rate that permeates through the membrane and A_m is the membrane area. Typical units for water flux in the literature include $m^3\,m^{-2}\,s^{-1}$, $m\,d^{-1}$, $\mu m\,s^{-1}$, $l\,m^{-2}\,h^{-1}$ and (US) gallons per ft^2 per day (gfd).

Similar to the definition of water flux, the mass flux of a solute J_s can be defined as the mass flow rate $\dot{m}_s$ passing through the membrane normalized by membrane area:

$$J_s = \frac{\dot{m}_s}{A_m} \qquad (6)$$

The solute flux is commonly given in $kg\,m^{-2}\,s^{-1}$, $kg\,m^{-2}\,h^{-1}$, $mol\,m^{-2}\,s^{-1}$, or $mol\,m^{-2}\,h^{-1}$.

The retention ability of a membrane in water applications is expressed by the membrane rejection. The intrinsic rejection of a membrane R_{int} can be defined as (Ho and Sirkar, 1992)

$$R_{int} = 1 - \frac{C_p}{C_m} \qquad (7)$$

where C_m is the solute concentration near the membrane surface and C_p is the solute concentration in the permeate water. Here, C_p can be determined from the ratio of the solute mass flux to the volumetric water flux by

$$C_p = \frac{J_s}{J_w} \qquad (8)$$

The intrinsic rejection R_{int} defined in Equation (7) relates the solute concentration in the permeate water C_p to that near the membrane surface C_m. Usually, C_m is not known as *a priori*.

Thus, a more commonly used rejection parameter in practice is the apparent rejection R_{app}, which relates C_p to the bulk feed concentration C_b (Ho and Sirkar, 1992):

$$R_{app} = 1 - \frac{C_p}{C_b} \qquad (9)$$

In a similar fashion, an overall observed rejection R_{sys} (rejection at the module or system level) can be defined based on the feedwater concentration C_f :

$$R_{sys} = 1 - \frac{C_p}{C_f} \qquad (10)$$

The overall rejection is usually lower than the intrinsic rejection. This can arise due to two main reasons: (1) concentration polarization which leads to a higher concentration near the membrane surface compared to the average bulk concentration ($C_m \geq C_b$), and/or (2) high membrane recovery so that the average bulk concentration experienced by a membrane is greater than the feedwater concentration ($C_b \geq C_f$). Thus, $R_{int} \geq R_{app} \geq R_{sys}$. The concentration polarization phenomenon will be discussed in greater detail in Section 4.11.6.3, and the effect of membrane recovery is discussed in Section 4.11.6.4.

It is also worth noting that the retention mechanism for porous membranes (MF and UF) is different from that for nonporous membranes (RO) (Table 11). Particles and solutes are retained by porous MF or UF membranes by size discrimination, that is, a sieving mechanism (Mulder, 1996). Particles larger than membrane pore size are completely retained, while smaller particles are less retained. In contrast, selectivity of an RO membrane is based the solution-diffusion mechanism (Mulder, 1996). Solute or solvent absorbs into the nonporous membrane on the feedwater side, diffuses through the rejection layer under a chemical potential gradient, and desorbs on the permeate water side. Separation of different species is achieved based on their different ability to partition into the rejection layer as well as their different ability to

Table 11 Rejection mechanisms for porous and nonporous membranes

Membrane type	Rejection layer	Rejection mechanism(s)	Water flux and solute rejection model(s)
MF	Porous	Sieving	Water flux: Hagen–Poiseuille equation; Kozeny–Carman equation Rejection: Ferry equation; Zeman and Wales equation; other pore models (Nakao, 1994)
UF	Porous	Sieving	Water flux: Hagen–Poiseuille equation; Kozeny–Carman equation Rejection: Ferry equation; Zeman and Wales equation; surface force-pore flow model; hindered transport models
NF	In between tight UF and loose RO	Solution-diffusion, sieving, Donnan exclusion	Solution-diffusion model; solution-diffusion-imperfection; preferential sorption-capillary flow model; surface force-pore flow model; Donnan equilibrium model; extended Nernst–Planck model
RO	Nonporous	Solution-diffusion	Solution-diffusion model; solution-diffusion-imperfection; preferential sorption-capillary flow model; surface force-pore flow model

MF, microfiltration; NF, nanofiltration; RO, reverse osmosis; UF, ultrafiltration.
Adapted from Schafer AI, Fane AG, and Waite TD (2005) *Nanofiltration – Principles and Applications*. Oxford: Elsevier; Ho WS and Sirkar KK (1992) *Membrane Handbook*. New York: Chapman and Hall; and Nakao S (1994) Determination of pore size and pore size distribution. 3. Filtration membranes. *Journal of Membrane Science* 96: 131–165.

diffuse through the rejection layer. RO membranes generally allow relatively high absorption of water molecules and faster diffusion of water molecules through the rejection layers (Mulder, 1996). In comparison, a typical solute (such as sodium chloride) has lower sorption onto RO membranes and slower diffusion through them, which results in a lower solute concentration in the permeate compared to that of the feedwater. As NF membranes are in between tight UF membranes and loose RO membranes, transport inside NF membranes may be governed by both solution-diffusion and sieving mechanisms (Schafer et al., 2005). In addition, charge repulsion (Donnan exclusion) can be important for the rejection of charged species (Schafer et al., 2005). Both porous membrane models and the solution-diffusion model are discussed in more detail in Section 4.11.6.2.

4.11.6.2   Transport Inside a Membrane – Basic Relationships

The permeate water flux of a membrane can be related to its driving force (i.e., the net pressure difference across the membrane) following the phenomenological Darcy's law:

$$J_w = L_p(\Delta P - \Delta\pi) \tag{11}$$

where L_p is the water permeability coefficient of the pressure-driven membrane.

In Equation (11), $\Delta\pi$ represents the osmotic pressure difference between the membrane surface π_m and permeate water π_p. The osmotic pressure of dilute solutions can be determined by the van't Hoff equation:

$$\pi = R_g T \sum C_i \tag{12}$$

where R_g is the universal gas constant ($R = 8.31\,J\,mol^{-1}\,K^{-1}$), T the absolute temperature in kelvin, and C_i the molar concentration of dissolved species i. Thus, for a 0.01 M NaCl, $\sum C_i = 0.02\,M$ as there are 0.01 M sodium ions (Na^+) and 0.01 M chloride ions (Cl^-). The osmotic pressure term appears in Equation (11) only if the solute under concern is retained by the membrane.

Similar to the osmotic pressure difference, ΔP in Equation (11) is the TMP, that is, the difference between the pressure near membrane surface P_m (which is identical to the applied pressure on the feedwater side) and that in the permeate water P_p. A positive TMP can be achieved by:

- applying a positive P_m while maintaining P_p around atmospheric pressure ($P_p \sim 0$); this is typically done for most RO and NF applications, as well as for many MF and UF applications and
- applying a negative P_p (suction or partial vacuum) while maintaining an atmospheric P_m, which is widely used for submerged membranes (see Section 4.11.5.2.4).

The Darcy's law for pressure-driven membranes is also commonly presented in terms of membrane hydraulic resistance R_m and dynamic viscosity of the permeating water η by

$$J_w = \frac{\Delta P - \Delta\pi}{\eta R_m} \tag{13}$$

where the membrane hydraulic resistance R_m is related to its water permeability by

$$R_m = \frac{1}{\eta L_p} \tag{14}$$

The Darcy's law (Equation (11) or Equation (13)) is applicable for both porous and nonporous membranes. A more sophisticated model available in the membrane literature is the irreversible thermodynamics model (Mulder, 1996; Bitter, 1991), which recognizes that membrane processes are not under thermodynamic equilibrium due to the continuous free energy dissipation and entropy production. According to the irreversible thermodynamics model, the volumetric flux J_v and the solute flux J_s are given by the following equations, respectively (Mulder, 1996; Bitter, 1991):

$$J_v = L_p(\Delta P - \sigma\Delta\pi) \tag{15}$$

and

$$J_s = \bar{C}(1 - \sigma)J_v + L_s\Delta C \tag{16}$$

where L_p is the water permeability, σ the reflection coefficient, $\bar{C}$ the average solute concentration inside the membrane, L_s the solute permeability coefficient, and ΔC the solute concentration across the membrane ($\Delta C = C_m - C_p$).

Equation (15) takes a similar form to that of Equation (11), except a reflection coefficient σ is introduced in the former. For $\sigma = 1$, two equations become identical. In effect, σ is an indicator of a membrane's ability to separate a solute from the solvent, and its value is usually between 0 and 1:

- For $\sigma = 0$, the membrane has no selectivity with respect to the solute. One example is the rejection of dissolved salts by porous membranes. As MF and (most) UF membranes do not retain dissolved salts, no osmotic pressure difference will be developed across these membranes (i.e., $\Delta\pi = 0$ and $\bar{C} = C_p = C_m$). This leads to $J_v = L_p\Delta P$ and $J_s = C_m J_v$. As a result of the complete leakage of solute, the volumetric flux only depends on the hydraulic pressure difference and the solute flux arises solely from convective transport.
- For $\sigma = 1$, the membrane has ideal separation properties so that the solute and the solvent transport through the membrane are independent and uncoupled to each other. As a result, the convective transport term (the first term in Equation (16)) is zero, and solute transport through the membrane is purely by diffusion. This leads to $J_v = L_p(\Delta P - \Delta\pi)$ and $J_s = L_s\Delta C$. A special example of this is rejection by high-retention RO membranes (Section 4.11.6.2.2).
- A real membrane typically has a σ between 0 and 1, which indicates that the solute transport is partially coupled to the solvent transport (Bitter, 1991).

The Darcy's law and the irreversible thermodynamic model treat a membrane as a black box. The effect of membrane structure and properties on the transport parameters (e.g., L_p and L_s) is not reflected in these models. For this reason, mechanistic models are preferred. Section 4.11.6.2.1 discusses transport models for porous MF and UF membranes, whereas Section 4.11.6.2.2 briefly reviews the solution-diffusion model commonly applied to RO membranes.

4.11.6.2.1 Transport models for MF and UF membranes

The water flux of MF and UF membranes can be described by the Hagen–Poiseuille equation for cylindrical-pore membranes or the Kozeny–Carman equation for stacked-sphere pore structure (refer to Section 4.11.2.3):

$$J_w \frac{\varepsilon r_p^2 \Delta P}{8 \eta \tau l_m} \quad \text{(Hagen−Poiseuille equation)} \qquad (17)$$

or

$$J_w = \frac{\varepsilon^3 \Delta P}{K(1-\varepsilon)^2 S^2 \eta l_m}$$
$$\text{(Kozeny−Carman equation)} \qquad (18)$$

The Hagen–Poiseuille equation and the Kozeny–Carman equation state that the water flux of a porous membrane is proportional to the applied pressure difference. The proportionality constant (i.e., the water permeability L_p) is a function of membrane pore structure (porosity, pore size, type of pores, etc.), the thickness of the rejection layer, and the viscosity of the permeating solution. The osmotic pressure difference $\Delta \pi$ does not appear in these models because MF and UF membranes do not retain dissolved salts so that their reflection coefficient σ is zero (refer to the irreversible thermodynamics model and Equation (15)). For some special cases where σ is not zero (e.g., osmotic pressure due to macromolecules that can be retained by UF membranes), the osmotic pressure difference term may need to be considered as well.

Rejection of solutes (or particles) by porous membranes is based on the sieving mechanism. A simple rejection equation based on Poiseuille flow for cylindrical-pore membranes was derived by Ferry (1936):

$$R_{int} = [\lambda(2-\lambda)]^2 \quad \text{(for } \lambda < 1) \qquad (19)$$

and

$$R_{int} = 1 \quad \text{(for } \lambda \geq 1) \qquad (20)$$

where λ is the ratio of solute (or particle) diameter to the pore diameter. Ferry's equation clearly suggests that rejection increases as the size of particle increases relative to the pore size.

Strictly speaking, Ferry's equation is applicable only for solid spherical particles in cylindrical pores. In addition, the interaction between particles in the pores and that between a particle and the pore wall are not considered. More sophisticated models are available in the literature (Ho and Sirkar, 1992; Nakao, 1994). Solute–solute and solute–pore interactions as well as membrane pore-size distribution are considered in some models (e.g., the surface force-pore flow model (Ho and Sirkar, 1992)).

4.11.6.2.2 Transport models for RO membranes

One of the most widely used transport models for RO membranes is the solution-diffusion model. This model assumes that (1) both the solvent and the solute absorb into the rejection layer and (2) they diffuse through the nonporous layer independent of each other under their respective chemical potential gradient. According to the solution-diffusion model, the water flux through an RO membrane is proportional to the net applied pressure ($\Delta P - \Delta \pi$), whereas the solute flux is proportional to the concentration difference across the membrane (ΔC):

$$J_w = A(\Delta P - \Delta \pi) \qquad (21)$$

and

$$J_s = B \Delta C \qquad (22)$$

where A and B are the respective water and solute permeability coefficients in the solution-diffusion model.

Comparing the solution-diffusion model and the irreversible thermodynamics model shows that the two models take the same form if the reflection coefficient σ is set to unity in Equations (15) and (16). The advantage of the solution-diffusion model is that the transport coefficients (A and B) in this model can be linked to membrane properties:

$$A = \frac{D_{wm} C_{wm} V_w}{R_g T l_m} \qquad (23)$$

and

$$B = \frac{D_{sm} K_{sm}}{l_m} \qquad (24)$$

where D_{wm} and D_{sm} are the diffusion coefficient of water and that of solute inside the rejection layer, respectively; C_{wm} the concentration of water inside the rejection layer; V_w the molar volume of water; and K_{sm} the solute partitioning coefficient into the rejection layer.

The solution-diffusion model suggests that a high-flux RO membrane shall have higher water absorption and also allow fast diffusion of water molecules (Equation (23)), which requires a lower degree of crosslinking of the rejection layer. However, reduced crosslinking will lead to a significantly enhanced diffusion of solutes and thus a much greater B value. This explains the strong trade-off relationship between water permeability and salt permeability for RO membranes, as discussed in Section 4.11.2.2.

The intrinsic rejection of an RO membrane can be determined by

$$R_{int} = \left(1 + \frac{B}{A(\Delta P - \Delta \pi)}\right)^{-1} \qquad (25)$$

As both A and B are inversely proportional to the rejection layer thickness l_m, the solution-diffusion model suggests that increasing rejection layer thickness alone does not improve membrane rejection. The intrinsic rejection of an RO membrane can be improved by (1) preferential sorption of water molecules compared to solute molecules, (2) enhanced diffusion of water molecules through the rejection layer relative to solute molecules, and (3) increased applied pressure.

The solution-diffusion model can be extended to include pore flows due to membrane imperfections (the solution-diffusion-imperfection model). Other models, such as the

preferential sorption-capillary flow model and the surface force-pore flow model, assume that the rejection layers of RO membranes are microporous. For NF membranes where electrostatic interaction is an important consideration, the Donnan equilibrium model and the extended Nernst–Planck model have also been applied. A review of these models is available (Ho and Sirkar, 1992; Schafer et al., 2005).

4.11.6.3 Transport toward a Membrane – Concentration Polarization

The solute concentration near a pressure-driven membrane surface is typically higher than the bulk concentration as a result of rejection by the membrane. The concentration gradient adjacent to the membrane surface leads to a diffusion of solute molecules back to the bulk solution. When the back diffusion balances with convective transport of solutes toward the membrane, a steady concentration polarization profile is established (Figure 21). Based on the mass balance of the solute in the control volume shown in Figure 21, the following equation can be established for describing the solute concentration C as a function of distance x for a one-dimensional problem:

$$J_w C - J_w C_p - D \frac{dC}{dx} = 0 \tag{26}$$

with the boundary conditions given by

$$C = C_b \quad \text{at} \quad x = 0 \tag{27}$$

and

$$C = C_m \quad \text{at} \quad x = \delta \tag{28}$$

J_w

C_m

$J_w C$

$D \dfrac{dC}{dx}$

$J_w C_p$

C_b
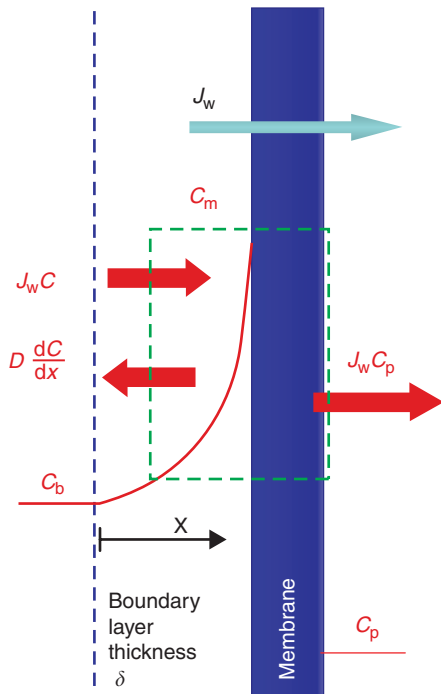
X

Boundary layer thickness δ

Membrane

C_p

Figure 21 Concentration polarization over a membrane surface.

Solving Equations (26)–(28) leads to

$$\frac{C_m - C_p}{C_b - C_p} = \exp(J_w/K) \tag{29}$$

where K is the mass transfer coefficient ($K = D/\delta$), and exp (J_w/K) is the concentration polarization modulus. Equation (29) is the boundary layer film model.

By substituting Equation (7) into Equation (29), we have

$$\frac{C_m}{C_b} = \frac{\exp(J_w/K)}{R_{int} + (1 - R_{int})\exp(J_w/K)} \tag{30}$$

For the special case where C_p is negligible (i.e., $R_{int} \sim 1$), Equation (30) becomes

$$\frac{C_m}{C_b} = \exp(J_w/K) \tag{31}$$

Equation (29) clearly shows that CP increases at higher water flux and reduced mass transfer coefficient. Thus, the membrane surface concentration C_m can be significantly higher than the bulk concentration at high flux and/or low mass transfer coefficient. The mass transfer coefficient can be determined from the Sherwood number Sh by relating Sh to Reynolds number Re and Schmidt number Sc (Table 12):

$$Sh = a \cdot Re^b Sc^c (d_h/L)^d \tag{32}$$

In Equation (32),

$$Sh = \frac{K d_h}{D} \tag{33}$$

$$Re = \frac{d_h u}{v} \tag{34}$$

$$Sc = \frac{v}{D} \tag{35}$$

where d_h is the hydraulic diameter, u the flow velocity, and v the kinetic viscosity.

Equation (32) can be rearranged to give the following form (assuming $c = 1/3$):

$$K = a \cdot D^{2/3} u^b v^{1/3-b} d_h^{b+d-1} L^{-d} \tag{36}$$

According to Equation (36), the mass transfer coefficient is proportional to $D^{2/3}$. This suggests that bigger molecules are more likely to suffer from severe concentration polarization as a result of their lower diffusion coefficient. Another important point is that the mass transfer coefficient can be enhanced at larger flow velocity in a crossflow module. However, this is usually at the expense of increased pressure drop across a membrane module (pressure difference between module inlet and outlet) (Ho and Sirkar, 1992; Schafer et al., 2005; Schock and Miquel, 1987). In addition, large crossflow may damage the membrane surface (such as formation of wrinkle structures). Typical crossflow velocities for SWMs are 10–90 cm s^{-1},

Table 12   Mass transfer correlations

Geometry	Flow region	Correlation	Notes
Channel or tube	Laminar	$Sh = 1.62 Re^{0.33} Sc^{0.33}(d_h/L)^{0.33}$	Fully developed flow ($L > 0.029 d_h$), $100 < Re\ Sc\ d_h/L < 5000$
		$Sh = 0.644 Re^{0.5} Sc^{0.33}(d_h/L)^{0.5}$	Developing flow ($L \leq 0.029 d_h$)
	Turbulent	$Sh = 0.023 Re^{0.8} Sc^{0.33}$	$Sc \leq 1$
		$Sh = 0.023 Re^{0.875} Sc^{0.25}$	$1 \leq Sc \leq 1000$
Stirred cell	Laminar	$Sh = 0.285 Re^{0.55} Sc^{0.33}$	$8000 \leq Re \leq 32\,000$
	Turbulent	$Sh = 0.044 Re^{0.75} Sc^{0.33}$	$32\,000 \leq Re \leq 82\,000$
Spacers filled channels	Laminar	$Sh = 0.644 Re^{0.5} Sc^{0.33}(d_h/L)^{0.5}$	Ladder type spacer (Da Costa *et al.*, 1994)
		$Sh = 0.644 k_{dc} Re^{0.5} Sc^{0.33}(2d_h/L)^{0.5}$	Diamond-type spacer, correction factor k_{dc} is a function of spacer geometry (Da Costa *et al.*, 1994)
	Turbulent	$Sh = 0.065 Re^{0.875} Sc^{0.25}$	Schock and Miquel (1987)

Adapted from Ho WS and Sirkar KK (1992) *Membrane Handbook*. New York: Chapman and Hall; and Fane AG (2005) Module design and operation. In: Schaefer AI, Fane AG, and Waite TD (eds.) *Nanofiltration – Principles and Applications*, pp. 67–88. Oxford: Elsevier.

while much higher crossflow velocities may be used for tubular modules due to their large tube diameter.

4.11.6.4   Factors Affecting Membrane Performance

The transport toward a membrane surface is discussed in Section 4.11.6.3 and that inside a membrane has been discussed in Section 4.11.6.2. By combining these two aspects together, the water flux and the apparent rejection of a membrane can be determined by

$$J_w = \frac{\Delta P - \exp(J_w/K)(\pi_b - \pi_p)}{\eta R_m} \qquad (37)$$

$$R_{app} = \frac{R_{int}}{R_{int} + (1 - R_{int})\exp(J_w/K)} \qquad (38)$$

Clearly, concentration polarization has a negative effect on both water flux and apparent rejection of a membrane; thus, J_w and R_{app} can be significantly reduced at higher CP modulus, $\exp(J_w/K)$. This effect is more severe for larger molecules at lower crossflow and higher flux (or higher applied pressure).

For systems or modules operated at low recovery (say recovery $Y < 0.1$), the average bulk concentration C_b in the membrane system can be approximated by the feedwater concentration C_f. However, C_b can be significantly larger than C_f for systems with high recovery. The reject water (e.g., brine in RO) concentration C_c can be determined by

$$C_c = C_f(1 - Y)^{-R_{app}} \qquad (39)$$

while the average bulk concentration in the system is approximated by

$$C_b \cong \frac{C_f \int_0^Y (1 - \Theta)^{-R_{app}} d\Theta}{Y} = C_f \frac{1 - (1 - Y)^{1-R_{app}}}{Y(1 - R_{app})}$$
$$(\text{for } 0 \leq R_{app} < 1 \text{ and } 0 < Y \leq 1) \qquad (40)$$

$$R_{sys} \cong 1 - \frac{1 - (1 - Y)^{1-R_{app}}}{Y} \qquad (41)$$

For typical applications, the feedwater concentration is given. Both the reject stream concentration and the average bulk concentration increase at higher recovery. Figure 22 shows the increase in rejection (brine) concentration and the correspondence osmotic pressure as a function of recovery for different feed concentration. For a feedwater containing 35 000 ppm NaCl (typical seawater conditions), the osmotic pressure of the brine is about 5.6 MPa at 50% recovery. Even for a feedwater with only moderate salt concentration (1000 ppm NaCl, typical wastewater reclamation conditions), this osmotic pressure can be substantial (~0.8 MPa at a recovery of 90%). As higher recovery increases the average bulk concentration and the corresponding osmotic pressure, this leads to reduced average flux as well as reduced system rejection (Equation (41)). For this reason, recovery for typical seawater RO desalination plants is limited to 50%, and that for wastewater reclamation plants is below 80%.

The effect of operating conditions (applied pressure, crossflow velocity, recovery, and temperature) on membrane performance is summarized below (Figure 23):

- *Applied pressure*. At low applied pressure (thus low flux level), concentration polarization is not significant. As applied pressure increases, water flux increases linearly initially according to the Darcy's law (Equation (37)). For a porous MF membrane, the solute rejection remains constant based on the Ferry model (Equation (19)). In contrast, the solute rejection also increases for RO based on the solution-diffusion model (Equation (25)). However, at high applied pressure and water flux, concentration polarization becomes important. Further increase in applied pressure will lead to a significant concentration polarization and thus significant increase in osmotic pressure. Such an increase in osmotic pressure can offset the increase in applied pressure, resulting in a significant deviation from the linear flux–pressure relationship. The increased membrane surface concentration will also result in lower apparent membrane rejection.
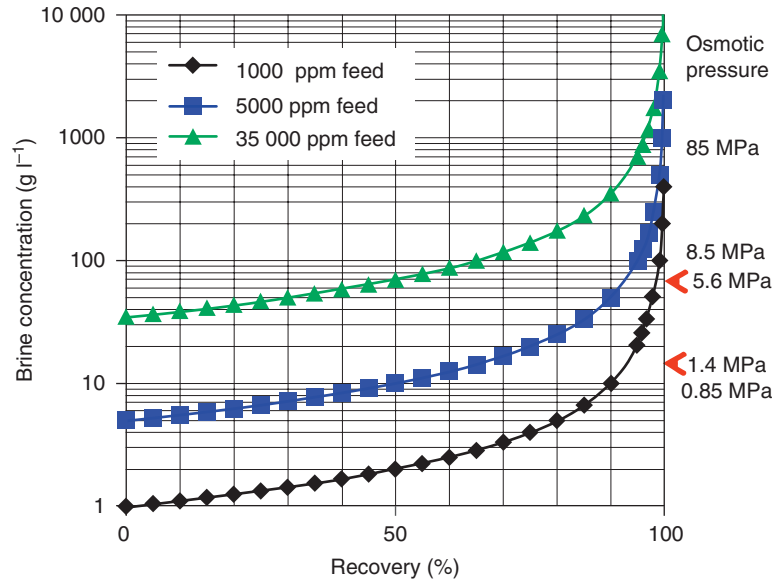
Figure 22 Brine concentration and osmotic pressure as a function of recovery for a high-retention RO membrane.
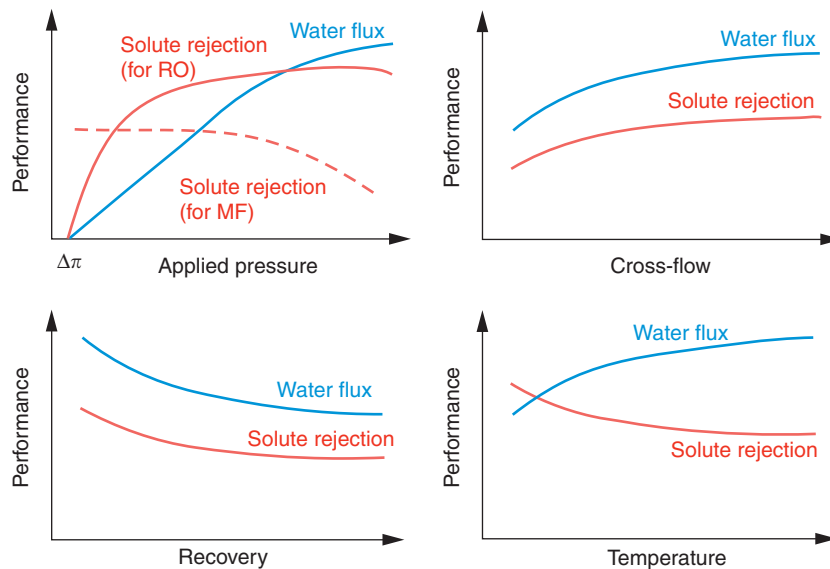

Figure 23 Effect of operating conditions on RO membrane performance. Adapted from Ho WS and Sirkar KK (1992) *Membrane Handbook*. New York: Chapman and Hall.

- *Crossflow velocity*. Increasing crossflow tends to improve both water flux and apparent rejection of a membrane as a result of reduced CP. A plateau is usually observed at high crossflow where further increase in crossflow velocity is less effective (mass transfer is no longer a limiting factor).
- *Recovery*. Increasing recovery leads to an increase in average bulk concentration. This reduces both water flux (due to increased osmotic pressure) and system rejection.
- *Temperature*. Higher operating temperature tends to increase both water flux and solute flux due to improved diffusion through the membrane rejection layer. However, the increase in solute flux is usually more drastic compared to the enhancement in water flux. Consequently, membrane rejection tends to decrease.

Besides the operating conditions mentioned above, membrane fouling can also have profound effect of the performance of a membrane. Fouling is discussed in more detail in Section 4.11.6.5.

4.11.6.5 Membrane Fouling

Membrane fouling is the deposition of contaminants on a membrane surface or inside membrane pores (**Figure 24**). According to the nature of the foulants, fouling can be classified into scaling (precipitation of insoluble salts), colloidal fouling, organic fouling, and biofouling (formation of a biofilm). Fouling leads to an additional hydraulic resistance (foulant resistance R_f) and therefore a lower water
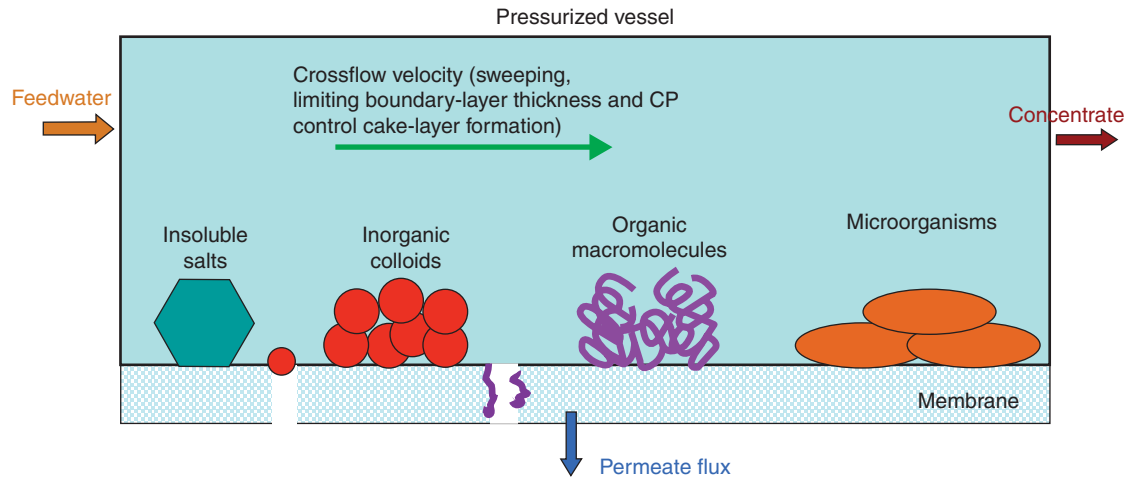
Figure 24 Illustration of membrane fouling in a pressurized crossflow module.

permeability of the fouled membrane:

$$J_w = \frac{\Delta P - \Delta \pi}{\eta(R_m + R_f)} \qquad (42)$$

The net effect of fouling is either reduced water flux at constant applied pressure or increased TMP to maintain a constant water flux. In either way, the energy demand to treat a unit volume of water can be increased significantly.

Both CP and fouling can reduce water flux during constant pressure operation. CP happens within the boundary layer near the membrane surface, and it is fully reversible. Once water flux is reduced to a low level, CP disappears. The timescale for CP to reach a stable condition or to disappear is usually very short (in seconds to a fraction of a minute (Chong et al., 2007)). In contrast, foulants attach onto a membrane during membrane fouling. Membrane fouling typically occurs over longer timescales (hours to days or months), although rapid fouling can happen under some unfavorable conditions. Although CP and fouling are two different phenomena, they are closely related to each other. Severe CP can accelerate membrane fouling as a higher foulant concentration is experienced by the membrane surface. On the other hand, the formation of a cake layer on membrane surface can potentially reduce the mass transfer coefficient which results in a severe cake enhanced concentration polarization (Chong et al., 2007).

Membrane fouling can be affected by many different factors, such as feedwater characteristics, membrane properties and module/system design, and hydrodynamic conditions over a membrane surface. In general, hydrophilic membranes with smooth surfaces have lower tendencies for fouling. A good module and system design improve mass transfer over the membrane surface (such as the use of spacer in SWMs and aeration in submerged membrane bioreactors (see Section 4.11.5)). Membrane fouling can be strongly affected by feedwater solution chemistry such as pH and ionic composition (Tang et al., 2007b). Unfavorable solution conditions (such as high ionic strength and hardness) can lead to severe colloidal and organic fouling by making membrane–foulant and foulant–foulant interactions less repulsive. Feedwater
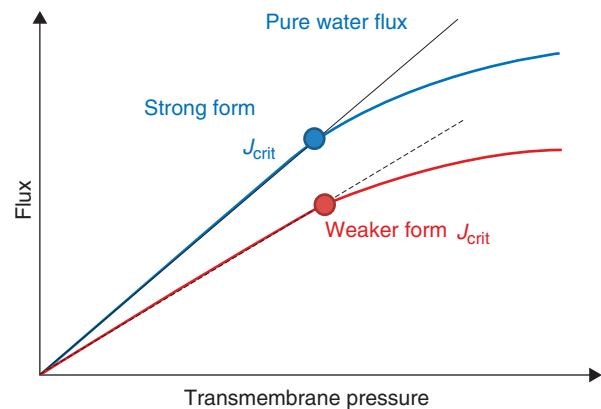

Figure 25 Critical flux in membrane operation. Modified from Bacchin P, Aimar P, and Field RW (2006) Critical and sustainable fluxes: Theory, experiments and applications. *Journal of Membrane Science* 281: 42–69.

contains high levels of sparingly soluble salts which are more susceptible to scaling formation, while the presence of microorganism and nutrients may promote biofouling. Pretreatment (such as removal of certain contaminants and pH adjustment) can be used to condition the feedwater for minimizing its fouling potential. Finally, hydrodynamic conditions are important for membrane fouling. Increased crossflow, thus enhanced mass transfer, helps minimize membrane fouling as well as CP. On the other hand, high membrane permeate flux tends to promote both CP and fouling problems.

The concept of critical flux has been widely used in the membrane fouling literature. The critical flux concept states that membrane fouling is minimal below a threshold flux value (the critical flux J_{crit}). Above the critical flux, significant fouling occurs. The theoretical basis has been extensively discussed in a review paper by Bacchin et al. (2006). In essence, the critical flux is the minimum flux needed to overcome the surface force and back diffusion of foulants such that fouling occurs. The critical flux can be classified into the strong form and weak form (Figure 25). In the strong form, the experimental flux versus TMP curve for a feedwater is compared to

its pure water flux curve, and the critical flux is the flux at which the experimental flux starts to deviate from the pure water flux. In its weak form, it is recognized that rapid surface or pore adsorption of macromolecules may occur which reduces the membrane permeability. Thus, the experimental flux in these cases is always below the pure water line. Nevertheless, the experimental flux is still linear with respect to the TMP over a wide range. The weaker form of critical flux is the flux at which the experimental flux starts to deviate from its linear trend (Figure 25). Subcritical flux operation is usually preferred to avoid successive membrane fouling. Membrane critical flux can be increased by increasing mass transfer rate (such as increasing crossflow velocity, bubbling, and vibration) and avoiding unfavorable solution conditions.

4.11.7 Membrane Process Operation

Membrane process operation requires consideration of whether the feed is delivered in crossflow or dead-end mode, and this depends on the nature and concentration of the contaminants to be removed. While the membranes (Sections 4.11.2 and 4.11.3) and the modules (Section 4.11.5) are the key components, the overall system includes pre- and posttreatment processes and various options for the arrangement of modules. The energy demand in most cases is directly related to the required input pressure and the fractional recovery (product/feed). The potential for energy recovery is significant in the high-pressure SWRO process. In the MBR, energy for air scour is important. The cost of water production using membranes has steadily fallen, and, in some cases, is equivalent to conventional processes.

4.11.7.1 Crossflow versus Dead-End Operation

In many membrane applications in the water industry, such as SWRO, RO reclamation, NF water treatment, and MBRs, the aim is to operate at a steady-state production rate with continuous crossflow for controlling concentration polarization (Section 4.11.6.3) and fouling (Section 4.11.6.5). In these applications, an important consideration is how the boundary layer is influenced by crossflow velocity which depends on the flow rates and the design of the module. Any membrane application where the feed fluid is caused to move tangentially to the membrane surface is in crossflow mode. For example, MBRs with submerged membranes are operated in crossflow mode, due to the effect of continuous air scouring that creates a two-phase flow across the membrane surface.

However, in the water industry, some applications are not operated in the crossflow mode. These include water treatment and pretreatment prior to RO. These processes use low-pressure membranes (MF and UF) and the feed streams have relatively low levels of suspended solids or turbidity. For these feeds, it is feasible to operate without continuous crossflow or surface shear, and this can reduce energy costs. This mode of operation is called dead-end filtration (or frontal filtration), and the key feature is that the deposition of retained species is allowed to grow. A typical cycle commences with a clean membrane (after backwash) and at constant imposed flux (J_i) the TMP rises according to Equation (43) (from Equation

(42), neglecting osmotic pressure):

$$\frac{\mathrm{d}\Delta P}{\mathrm{d}t} = \eta J_i \frac{\mathrm{d}R_f}{\mathrm{d}t} \qquad (43)$$

After a specified period, t_c, or at a predetermined maximum pressure drop, the flux is stopped and the deposit is removed by backwashing and (usually) vigorous aeration. The cycle times would typically be about 30 min and the backwash <5 min. This mode of operation is batch-continuous, and net flux would be slightly less than the imposed flux, that is, for t_c of 30 min and for t_{BW} of 5 min, the net flux is about 80% of imposed flux (allowing for loss of product in backwash water). Over time, due to fouling, a residual resistance may build up. This can usually be controlled by a cleaning cycle, such as chemically enhanced backwash.

4.11.7.2 System Components

Membrane process systems comprise membranes and modules as key components. Important additional components are the intake systems, the pretreatment steps, the feed pumps, the posttreatment steps, the energy recovery devices, and concentrate disposal method. Figure 2 is a simplified flow sheet of membrane process configurations in the water industry and Table 2 summarizes the pre- and posttreatment steps involved. Other ancillary components could be chemical addition to control fouling, membrane cleaning systems, and
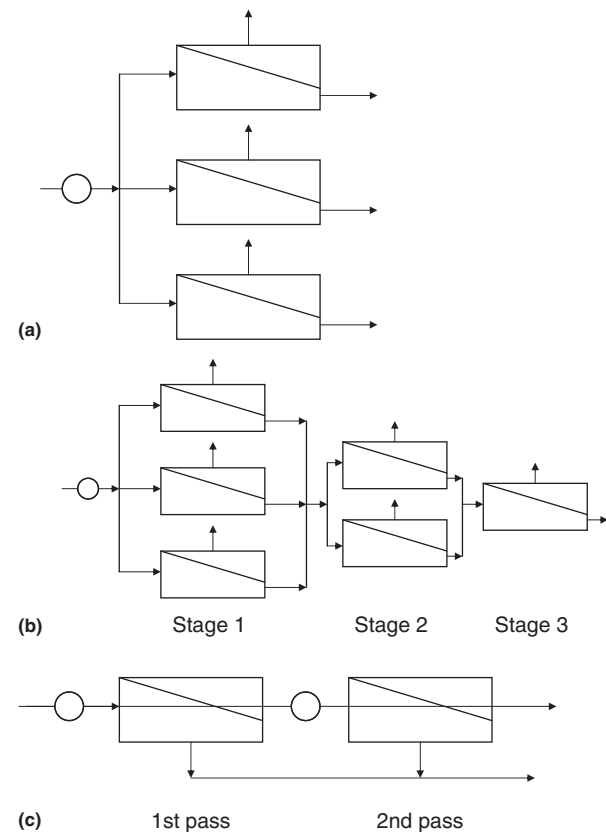

Figure 26 (a) Parallel connection. (b) Tapered cascade 3:2:1 array. (c) Two pass connection.

Table 13 Approximate energy demand and costs for membrane applications to water industry

Membrane application	Energy demand (kWh m^{-3})	Production cost (USD m^{-3})	Reference
Seawater RO	3.2–3.8	0.5–0.75	Voutchkov and Semiat (2008)
RO reclamation	1.0–1.5	~0.3	Cote et al. (2008)
MBR	<0.8	Similar to conventional	Cornel and Krause (2008)
Water treatment	<0.3	Similar to conventional	

MBR, membrane bioreactor; RO, reverse osmosis.

integrity testing facilities. Integrity tests are important in water treatment to check if damaged fibers are present. One popular test is the air pressure decay test (a damaged fiber shows rapid pressure loss) (Kennedy et al., 2008).

Membrane modules can be connected in various ways, in series and parallel, as depicted in Figure 26. The low-pressure applications tend to have modules connected in parallel with permeate taken to a common header (Figure 26(a)). The feed is similar to all modules, although in a large system the feed may be staged. In a typical SWRO plant, the modules are arranged in both series and parallel (Figure 26(b)). The first-stage pressure vessels are connected in parallel, the number of paths depending on the maximum allowable flow per module. Within the pressure vessel there would be 6–8 SWMs connected in series, such that toward the vessel outlet, the concentration builds up and the flow drops due to permeate removal. The process is continued in the second and possibly third-stage pressure vessels as shown in Figure 26(b). In this example, the second and third stages have fewer vessels in parallel as the net volumetric flow has dropped; this is known as a tapered cascade and the example is a 3:2:1 cascade. The permeate from the stages is often blended. Feed pumps may be augmented by interstage pumps to maintain pressure-driving force along the cascade.

Another option is depicted in Figure 26(c), which shows a two-pass arrangement with permeate from the first set of membranes having further treatment in a second set of membranes. This approach is used if there is a need for greater removals of specific contaminants, such as boron.

4.11.7.3 Energy and Economic Issues

Energy demand and production costs are important parameters for the water industry. As can be anticipated the greater the required pressure or the more fouling the feed, the greater the energy demand and cost. This means that energy and cost ranking is in the order, SWRO > RO reclamation > MBR > water treatment.

A guide to the intrinsic energy demand can be obtained by noting for a flow of Q (m^3 s^{-1}), with feed pressure P (Pa or N m) and a recovery Y (volume product/volume feed) the energy demand is $QP/QY = (P/Y) \times (1/3.6 \times 10^6)$ (correcting W s m^{-3} to kWh m^{-3}). For SWRO operating at a feed pressure of 70 bar and recovery of 0.5, the intrinsic energy usage can be estimated as 3.9 kWh m^{-3}. However, modern RO plants use pressure energy recovery on the brine stream which could return about 1.7 kWh m^{-3}, giving a net energy of about 2.2 kWh m^{-3}. Even lower values have been achieved for SWRO under carefully optimized conditions, with a value of

1.56 kWh m^{-3} reported (Truby, 2008). It should be noted that these values are for the RO stage only and it is usual to report plant data including seawater intake pumps, pretreatment, and other miscellaneous plant energy use. These add 0.6–1.0 kWh m^{-3} to energy demand (Voutchkov and Semiat, 2008). Table 13 summarizes typical energy data.

The energy demand for RO reclamation is significantly less than SWRO, due to the much lower pressures required (about one-fourth of SWRO). Based on differences in O and M costs (Cote et al., 2008), the energy demand would be less than 50% of SWRO. For the MBR, a major energy demand is air scour to control fouling. Typical energy demand for MBR processing municipal wastewater is 0.75–1.0 kWh m^{-3} (Cornel and Krause, 2008) and developments promise lower energy usage. Finally, treatment of surface water by membranes, using dead-end with backwash, has a modest energy demand of typically <0.3 kWh m^{-3}.

Production costs follow similar trends to the energy demands. Table 13 gives indicative costs. It should be noted that the range could be considerable and depends on scale of operation (small plant typically have more costly product). SWRO is most costly, but the cost of production is only <0.1 cents US per liter. RO reclamation delivers water at about 50% of the cost of SWRO. For the low-pressure processes, it is now evident that both the MBR and membrane water treatment have similar costs to conventional processes for green field sites. The marginally higher energy costs are offset by the smaller foot print and infrastructure costs.

4.11.8 Conclusions

Membrane technology is playing an increasingly significant role in the water industry. Membranes are applied across the spectrum from seawater desalination, through wastewater treatment and reclamation, to surface water treatment. The technology continues to advance with improved membranes and processes. The energy demands and production costs have steadily declined and, in some cases, are similar to conventional processes, but with better-quality water products.

References

Aimar P, Meireles M, and Sanchez V (1990) A contribution to the translation of retention curves into pore size distributions for sieving membranes. *Journal of Membrane Science* 54: 321–338.

Bacchin P, Aimar P, and Field RW (2006) Critical and sustainable fluxes: Theory, experiments and applications. *Journal of Membrane Science* 281: 42–69.

Birkett J and Truby R (2007) A figure of merit for appreciating improvements in RO membrane performance. *International Desalination Association News* 16(1–2): 2–3.

Bitter JGA (1991) *Transport Mechanisms in Membrane Separation Processes*. New York: Plenum.

Bowen WR, Hilal N, Lovitt RW, and Wright CJ (1999) Characterization of membrane surfaces: Direct measurement of biological adhesion using an atomic force microscope. *Journal of Membrane Science* 154: 205–212.

Cadotte JE (1977) Reverse Osmosis Membranes. US Pat. 4,039,440, 2 August 1977.

Childress AE and Elimelech M (1996) Effect of solution chemistry on the surface charge of polymeric reverse osmosis and nanofiltration membranes. *Journal of Membrane Science* 119: 253–268.

Childress AE and Elimelech M (2000) Relating nanofiltration membrane performance to membrane charge (electrokinetic) characteristics. *Environmental Science and Technology* 34: 3710–3716.

Chong TH, Wong FS, and Fane AG (2007) Fouling in reverse osmosis: Detection by non-invasive techniques. *Desalination* 204: 148–154.

Cornel P and Krause S (2008) Membrane bioreactors for wastewater treatment. In: Li NN, Fane AG, Ho WSW, and Matsuura T (eds.) *Advanced Membrane Technology and Applications*, pp. 217–238. Hoboken, NJ: Wiley.

Coster HGL, Chilcott TC, and Coster ACF (1996) Impedance spectroscopy of interfaces, membranes and ultrastructures. *Bioelectrochemistry and Bioenergetics* 40: 79–98.

Cote P, Liu M, and Siverns S (2008) Water reclamation and desalination by membranes. In: Li NN, Fane AG, Ho WSW, and Matsuura T (eds.) *Advanced Membrane Technology and Applications*, pp. 171–188. Hoboken, NJ: Wiley.

Da Costa AR, Fane AG, and Wiley DE (1994) Spacer characterization and pressure drop modelling in spacer-filled channels for ultrafiltration. *Journal of Membrane Science* 87: 79–98.

Fane AG (2005) Module design and operation. In: Schaefer AI, Fane AG, and Waite TD (eds.) *Nanofiltration-Principles and Applications*, pp. 67–88. Oxford: Elsevier.

Fane AG (2008) Submerged membranes. In: Li NN, Fane AG, Ho WSW, and Matsuura T (eds.) *Advanced Membrane Technology and Applications*, pp. 239–270. Hoboken, NJ: Wiley.

Ferry JD (1936) Statistical evaluation of sieve constants in ultrafiltration. *Journal of General Physiology* 20: 95–104.

Freger V, Bottino A, Capannelli G, Perry M, Gitis V, and Belfer S (2005) Characterization of novel acid-stable NF membranes before and after exposure to acid using ATR-FTIR, TEM and AFM. *Journal of Membrane Science* 256: 134–142.

Hagg MB (2008) Membranes in gas separations. In: Pabby AK, Rizvi SSH, and Sastre AM (eds.) *Handbook of Membrane Separations: Chemical, Pharmaceutical and Biotechnological Applications*, pp. 65–107. Boca Raton, FL: CRC Press.

Ho WS and Sirkar KK (1992) *Membrane Handbook*. New York: Chapman and Hall.

Jeong B-H, Hoek EMV, and Yan Y (2007) Interfacial polymerization of thin film nanocomposites: A new concept for RO membranes. *Journal of Membrane Science* 294(1–2): 1–7.

Jones KL and O'Melia CR (2000) Protein and humic acid adsorption onto hydrophilic membrane surfaces: Effects of pH and ionic strength. *Journal of Membrane Science* 165: 31–46.

Judd S (2006) *The MBR Book*. Oxford: Elsevier.

Kennedy MD, Kamanyi J, Salinas SS, Lee NH, Schippers JC, and Amy G (2008) Water treatment by microfiltration and ultrafiltration. In: Li NN, Fane AG, Ho WSW, and Matsuura T (eds.) *Advanced Membrane Technology and Applications*, pp. 131–170. Hoboken, NJ: Wiley.

Kesting RE (1985) Phase inversion membranes. In: Lloyd DR (ed.) *Materials Science of Synthetic Membranes, ACS Symposium Series*, vol. 269, ch. 7, pp. 131–164. Washington, DC: American Chemical Society.

Khayet H (2008) Membrane distillation. In: Li NN, Fane AG, Ho WSW, and Matsuura T (eds.) *Advanced Membrane Technology and Applications*, pp. 297–370. Hoboken, NJ: Wiley.

Khedr MG (2003) Development of reverse osmosis desalination membranes composition and configuration: Future prospects. *Desalination* 153: 295–304.

Kim KJ, Fane AG, Fell CJD, Suzuki T, and Dickson MR (1990) Quantitative microscopic study of surface characteristics of ultrafiltration membranes. *Journal of Membrane Science* 54: 89–102.

Kimura K, Amy G, Drewes JE, Heberer T, Kim TU, and Watanabe Y (2003) Rejection of organic micropollutants (disinfection by-products, endocrine disrupting compounds, and pharmaceutically active compounds) by NF/RO membranes. *Journal of Membrane Science* 227: 113–121.

Kumano A and Fujiwara N (2008) Cellulose triacetate membranes for reverse osmosis. In: Li NN, Fane AG, Ho WSW, and Matsuura T (eds.) *Advanced Membrane Technology and Applications*, pp. 21–46. Hoboken, NJ: Wiley.

Kwon YN, Tang CY, and Leckie JO (2006) Change of membrane performance due to chlorination of crosslinked polyamide membranes. *Journal of Applied Polymer Science* 102: 5895–5902.

Kwon YN, Tang CY, and Leckie JO (2008) Change of chemical composition and hydrogen bonding behavior due to chlorination of crosslinked polyamide membranes. *Journal of Applied Polymer Science* 108: 2061–2066.

Lebeau T, Lelievre C, Buisson H, Cleret D, De Venter LWV, and Cote P (1998) Immersed membrane filtration for the production of drinking water: Combination with PAC for NOM and SOCs removal. *Desalination* 117: 219–231.

Le-Clech P, Chen V, and Fane AG (2006) Fouling in membrane bioreactors used in wastewater treatment: A review. *Journal of Membrane Science* 284(1–2): 17–53.

Lee S and Elimelech M (2006) Relating organic fouling of reverse osmosis membranes to intermolecular adhesion forces. *Environmental Science and Technology* 40: 980–987.

Li K (2007) *Ceramic Membranes for Separation and Reaction*. Chichester: Wiley.

Lieknes TO (2009) Wastewater treatment by membrane bioreactors. In: Drioli E and Giorno L (eds.) *Membrane Operations, Innovative Separations and Transformations*, pp. 363–396. Weinheim: Wiley-VCH.

Liu LH, Gao SJ, Yu YH, Wang R, Liang DT, and Liu M (2006) Bio-ceramic hollow fiber membranes for immunoisolation and gene delivery – I: Membrane development. *Journal of Membrane Science* 280: 375–382.

Loeb S and Sourirajan S (1964) High Flow Semipermeable Membrane for Separation of Water from Saline Solutions. US Pat. 3,133,132, 12 May 1964.

Louie JS, Pinnau I, Ciobanu I, Ishida KP, Ng A, and Reinhard M (2006) Effects of polyether-polyamide block copolymer coating on performance and fouling of reverse osmosis membranes. *Journal of Membrane Science* 280: 762–770.

Mahon HI (1966) Permeability Separatory Apparatus and Membrane Element, Method of Making the Same and Process Ultilizing the Same. US Pat. 3228876, 11 January 1966.

Mckelvey SA, Clausi DT, and Koros WJ (1997) A guide to establishing hollow fiber macroscopic properties for membrane applications. *Journal of Membrane Science* 124: 223.

Mulder M (1996) *Basic Principles of Membrane Technology*, 2nd edn. Dordrecht: Kluwer.

Nakao S (1994) Determination of pore size and pore size distribution. 3. Filtration membranes. *Journal of Membrane Science* 96: 131–165.

Pearce G (2007) Introduction to membranes: Membrane selection. *Filtration and Separation* 44: 35–37.

Petersen RJ (1993) Composite reverse-osmosis and nanofiltration membranes. *Journal of Membrane Science* 83: 81–150.

Qin JJ, Wang R, and Chung TS (2001) Investigation of shear stress effect within a spinneret on flux, separation and thermomechanical properties of hollow fiber ultrafiltration membranes. *Journal of Membrane Science* 175: 197.

Ren JZ and Wang R (2010) Preparation of polymeric membranes. In: Wang LK, Chen JP, Hung YT, and Shammas NK (eds.) *Handbook of Environmental Engineering*, vol. 13, ch. 2. Totowa, NJ: Humana Press (in press).

Schafer AI, Fane AG, and Waite TD (2005) *Nanofiltration – Principles and Applications*. Oxford: Elsevier.

Schock G and Miquel A (1987) Mass transfer and pressure loss in spiral wound modules. *Desalination* 64: 339–352.

Seah H, Tan TP, Chong ML, and Leong J (2008) NEWater – multi safety barrier approach for indirect potable use. *Water Science and Technology* 8(5): 573–588.

Shi L, Wang R, Cao YM, Liang DT, and Tay JH (2008) Effect of additives on the fabrication of poly(vinylidene fluoride-*co*-hexafluropropylene) (PVDF-HFP) asymmetric microporous hollow fiber membranes. *Journal of Membrane Science* 315: 195–204.

Strathmann H (1990) Synthetic membranes and their preparation. In: Porter M (ed.) *Handbook of Industrial Membrane Technology*, pp. 1–60. Park Ridge, NJ: Noyes Publications.

Tang CY and Leckie JO (2007) Membrane independent limiting flux for RO and NF membranes fouled by humic acid. *Environmental Science and Technology* 41: 4767–4773.

Tang CY, Kwon YN, and Leckie JO (2007a) Probing the nano- and micro-scales of reverse osmosis membranes – a comprehensive characterization of physiochemical properties of uncoated and coated membranes by XPS, TEM, ATR-FTIR, and streaming potential measurements. *Journal of Membrane Science* 287: 146–156.

Tang CY, Kwon YN, and Leckie JO (2007b) Fouling of reverse osmosis and nanofiltration membranes by humic acid – effects of solution composition and hydrodynamic conditions. *Journal of Membrane Science* 290: 86–94.

Tang CY, Kwon YN, and Leckie JO (2009a) Effect of membrane chemistry and coating layer on physiochemical properties of thin film composite polyamide RO and NF membranes II. Membrane physiochemical properties and their dependence on polyamide and coating layers. *Desalination* 242: 168–182.

Tang CY, Kwon YN, and Leckie JO (2009b) Effect of membrane chemistry and coating layer on physiochemical properties of thin film composite polyamide RO and NF membranes. I. FTIR and XPS characterization of polyamide and coating layer chemistry. *Desalination* 242: 149–167.

Tang CY, Kwon YN, and Leckie JO (2009c) The role of foulant–foulant electrostatic interaction on limiting flux for RO and NF membranes during humic acid fouling-theoretical basis, experimental evidence, and AFM interaction force measurement. *Journal of Membrane Science* 326: 526–532.

Truby R (2008) Seawater desalination by ultralow-energy reverse osmosis. In: Li NN, Fane AG, Ho WSW, and Matsuura T (eds.) *Advanced Membrane Technology and Applications*, pp. 87–100. Hoboken, NJ: Wiley.

Voutchkov N and Semiat R (2008) Seawater desalination. In: Li NN, Fane AG, Ho WSW, and Matsuura T (eds.) *Advanced Membrane Technology and Applications*, pp. 47–86. Hoboken, NJ: Wiley.

Vrijenhoek EM, Hong S, and Elimelech M (2001) Influence of membrane surface properties on initial rate of colloidal fouling of reverse osmosis and nanofiltration membranes. *Journal of Membrane Science* 188: 115–128.

Wittmann E and Thorsen T (2005) Water treatment. In: Schaefer AI, Fane AG, and Waite TD (eds.) *Nanofiltration-Principles and Applications*, pp. 263–286. Oxford: Elsevier.